Mitochondria-targeted melatonin photorelease supports the presence of melatonin MT1 receptors in mitochondria inhibiting respiration

Gloria Somalo Barranco [1,2], Antonio Pagano-Zottola [3], Abdulrasheed Abdulrahman[1], Rami El Zein[1], Astrid Cannich[3], Lourdes Muñoz [2,4], Carme Serra [2,4], Atsuro Oishi [1], Giovanni Marsicano [3], Bernard Masri [1], Luigi Bellocchio [3], Amadeu Llebaria [2, 5,*] and Ralf Jockers [1, 5, 6, *]

[1] Université de Paris, Institut Cochin, INSERM, CNRS, F-75014 PARIS, France

[2] MCS, Laboratory of Medicinal Chemistry & Synthesis, Department of Biological Chemistry, Institute for Advanced Chemistry of Catalonia (IQAC-CSIC), Barcelona, Spain

[3] INSERM, U1215 NeuroCentre Magendie, Endocannabinoids and Neuroadaptation, Bordeaux, France

[4] SIMChem, Synthesis of High Added Value Molecules, Institute of Advanced Chemistry of Catalonia (IQAC-CSIC), Barcelona, Spain

[5] Co-senior authors

[6] Lead contact

[*] Correspondence: ralf.jockers@inserm.fr (R.J)., amadeu.llebaria@iqac.csic.es (A.L.)

Running title: mitochondria-targeting caged melatonin ligands

Summary

The presence of signaling-competent G protein-coupled receptors in intracellular compartments is increasingly recognized. Recently, the presence of $G_{i/o}$ protein-coupled melatonin MT_1 receptors in mitochondria has been revealed, in addition to the plasma membrane. Melatonin is highly cell-permeant, activating plasma membrane and mitochondrial receptors equally. Here, we present MCS-1145, a melatonin derivative bearing a triphenylphosphonium cation for specific mitochondrial targeting and a photocleavable *o*-nitrobenzyl group that releases melatonin upon illumination. MCS-1145 displayed low affinity for MT_1 and MT_2 but spontaneously accumulated in mitochondria, where it was resistant to washout. Uncaged MCS-1145 and exogenous melatonin inhibited oxygen consumption in mitochondria isolated from HEK293 cells expressing MT_1, but not in mock or MT_2-expressing cells. Similar effects were observed in mitochondria isolated from mouse cerebellum of WT mice but not from MT_1 knockout mice. Overall, we developed the first mitochondria-targeted photoactivatable melatonin ligand and demonstrate that melatonin inhibits mitochondrial respiration through mitochondrial MT_1 receptors.

Keywords: melatonin, melatonin receptors, mitochondria-targeted caged melatonin ligand, photopharmacology, mitochondrial respiration

Introduction

Melatonin (5-methoxy-*N*-acetyltryptamine) is a hormone that is primarily synthesized in the pineal gland and the retina, following a circadian rhythm with high levels throughout the night (Dubocovich et al., 2010). It regulates a wide variety of physiological functions in the body, such as sleep, biological rhythms, immune responses, retinal physiology, pain and neuroendocrine processes (Liu et al., 2016). These effects are mediated through the activation of MT_1 and MT_2 receptors, which are members of the G protein-coupled receptor (GPCR) family (Jockers et al., 2016). Both melatonin receptors primarily couple to proteins of the $G_{i/o}$ subfamily, MT_1 couples in addition to G_{12} and G_{15} and MT_2 to G_z (Hegron et al., 2021; Karamitri et al., 2018). Coupling to $G_{q/11}$ proteins is also observed but depends on the cellular context (Chen et al., 2020b). Both receptors recruit β-arrestin1/2 (Hegron et al., 2021; Karamitri et al., 2018). In humans, MT_1 and MT_2 receptors are expressed in distinct brain regions such as the hypothalamus and the cerebellum and several peripheral organs, including the retina, fetal kidney and adipose tissue (Cecon et al., 2018).

Along with other GPCRs, melatonin receptors are well-known cell-surface receptors that transmit extracellular signals into cells. Increasing evidence supports the ability of GPCRs to promote also signaling from intracellular compartments as diverse as endosomes, the Golgi, mitochondria and the nuclear membrane (Jong et al., 2018; Mohammad Nezhady et al., 2020; Tsvetanova et al., 2015; Vilardaga et al., 2014). The MT_1 receptor is an interesting model receptor in this context as this receptor, in addition to its plasma membrane localization, was identified in brain mitochondria, where this receptor is postulated to be involved in neuroprotection (Suofu et al., 2017; Wang et al., 2011). The molecular function of mitochondrial MT_1 are poorly understood, solely an inhibitory effect on stress-mediated cytochrome c release from mitochondria was suggested (Suofu et al., 2017). The natural ligand, melatonin, reaches and activates both cell surface and mitochondrial receptors equally due to its lipophilic nature and high permeability. Selective activation of cell surface MT_1 can be achieved with the cell-

impermeant melatonin receptor agonist ICOA-13 (Gbahou et al., 2017). In contrast, compounds solely acting on mitochondrial MT_1 receptors are not available to study specific organelle effects. Therefore, it would be desirable to develop a molecular tool to study the activation of mitochondrial MT_1 by the endogenous melatonin ligand. In addition to the receptor-dependent effects, a delimited delivery of melatonin in mitochondria could be also useful to investigate with high spatiotemporal control other, receptor-independent, effects suspected to be mediated by melatonin in mitochondria such as the redox status and antioxidant properties (Melhuish Beaupre et al., 2021; Reiter et al., 2017; Yang et al., 2013).

We report here the design, synthesis and validation of **MCS-1145**, a compound that selectively accumulates in mitochondria and releases biologically active melatonin upon light-activation. We show that **MCS-1145** and melatonin inhibit the oxygen consumption rate of mitochondria isolated from MT_1-expressing HEK293 cells and cerebellum lysates of C57bl/6 mice but not from mock-transfected or MT_2-expressing HEK293 cells or from cerebellum lysates of MT_1 knockout (KO) mice, respectively.

Results

Design and chemical synthesis of MCS-1145.

The chemical design of **MCS-1145** was based on the previously described compound **MCS-0382** which is composed of melatonin attached at its indolic nitrogen to an *o*-nitrobenzyl (*o*-NB) photocleavable group (Somalo-Barranco et al., 2022). This *o*-NB caging group drastically reduces the affinity the compound for melatonin receptors and allows controlled generation of biologically active melatonin by applying light, which promotes uncaging through a photolytic reaction (Somalo-Barranco et al., 2022). Here, we developed **MCS-1145**, a new derivative containing a triphenylphosphonium cation (TPP^+) group, intended to accumulate selectively in mitochondria (Burns et al., 1995; Zielonka et al., 2017) and to photorelease melatonin in this specific subcellular compartment. This strategy has been already successfully used for several

photoactivable molecules to promote mitochondria-specific release of the active molecule (Chalmers et al., 2012; Farley et al., 2021; Feng et al., 2018; Wagner et al., 2018). As we intended to produce melatonin from an inactive precursor, we selected to add the mitochondria targeting TPP^+ moiety to the 4,5-dimethoxy-2-nitrobenzyl (DMNB) present in **MCS-0382** (**Figure 1**), with the idea to maintain the good performance of this compound in melatonin photorelease. Accordingly, we selected one of the methoxy groups in the DMNB, and TPP^+ was attached with an alkyl linker, to specifically accumulate the compound in mitochondria (**Figure 1**).

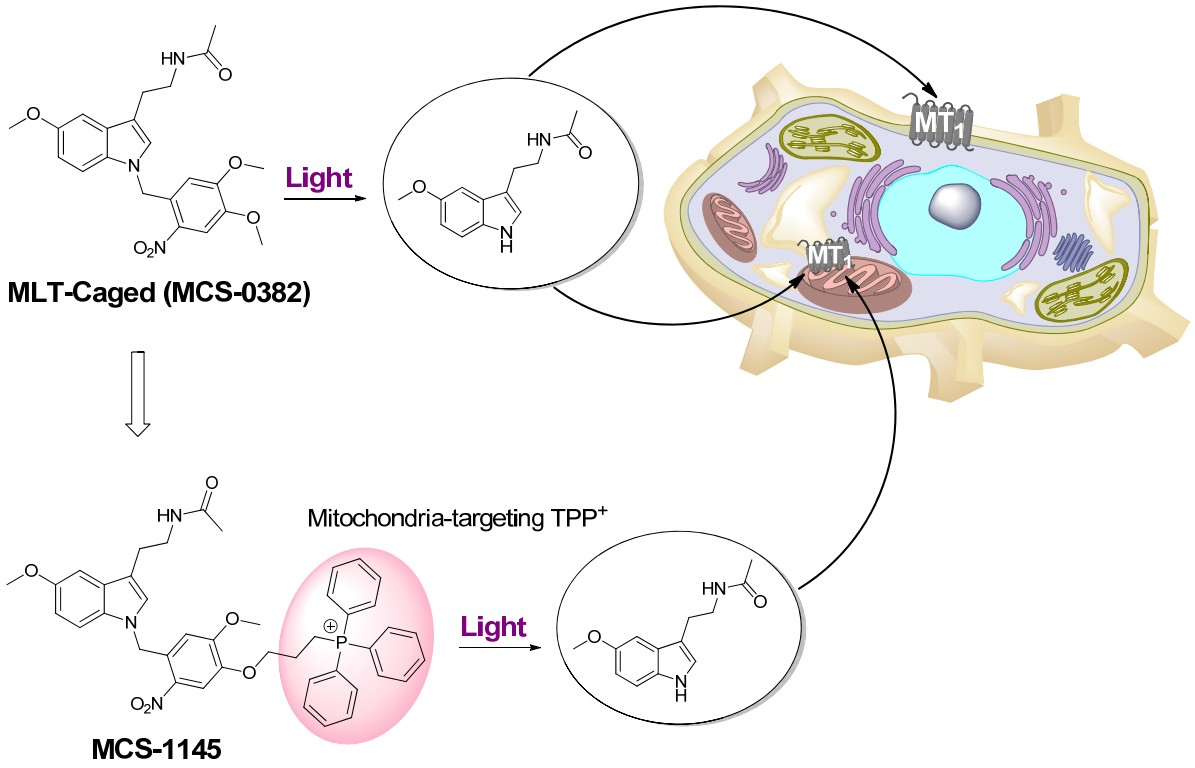

Figure 1. Chemical design of the mitochondria-targeted **MCS-1145**. Based on the photo-activable caged compound for melatonin receptors **MCS-0382**, a mitochondria-targeted moiety, TPP^+, is attached to its chemical structure through an alkyl linker, resulting in compound **MCS-1145**.

The synthetic pathway to obtain mitochondria-targeted compound **MCS-1145** is depicted in **Figure 2**. Steps **a** to **d** followed a modified procedure from Lai et al., 2016, starting with commercially available vanillin **1** to obtain derivative **5**. Initial protection of the phenol with a benzyl group gave compound **2**. This step was followed by a nitration, yielding the light-

sensitive *o*-nitrobenzaldehyde **3**. Deprotection and reduction of the aldehyde gave benzyl alcohol **5**, which was transformed into the bromide **6** by a regioselective alkylation at the phenolic oxygen in **5**. The benzyl alcohol was then converted to benzyl bromide by following previous procedures (Paul et al., 2016), yielding compound **7** in moderate yields. The intermediate dibromide **8** was obtained after deprotonation of melatonin with sodium hydride (NaH), followed by the rapid addition of **7** at low temperature. The double addition of melatonin at both bromide positions of **7** was detected as the main product in step **g**. Attempts to induce a selective monoalkylation at benzylic carbon were unsuccessful. Finally, compound **8** was finally isolated, albeit in low yields, but in sufficient amounts to perform a nucleophilic substitution with triphenylphosphine (TPP) to give the mitochondria-targeting compound **MCS-1145** (75% yield).

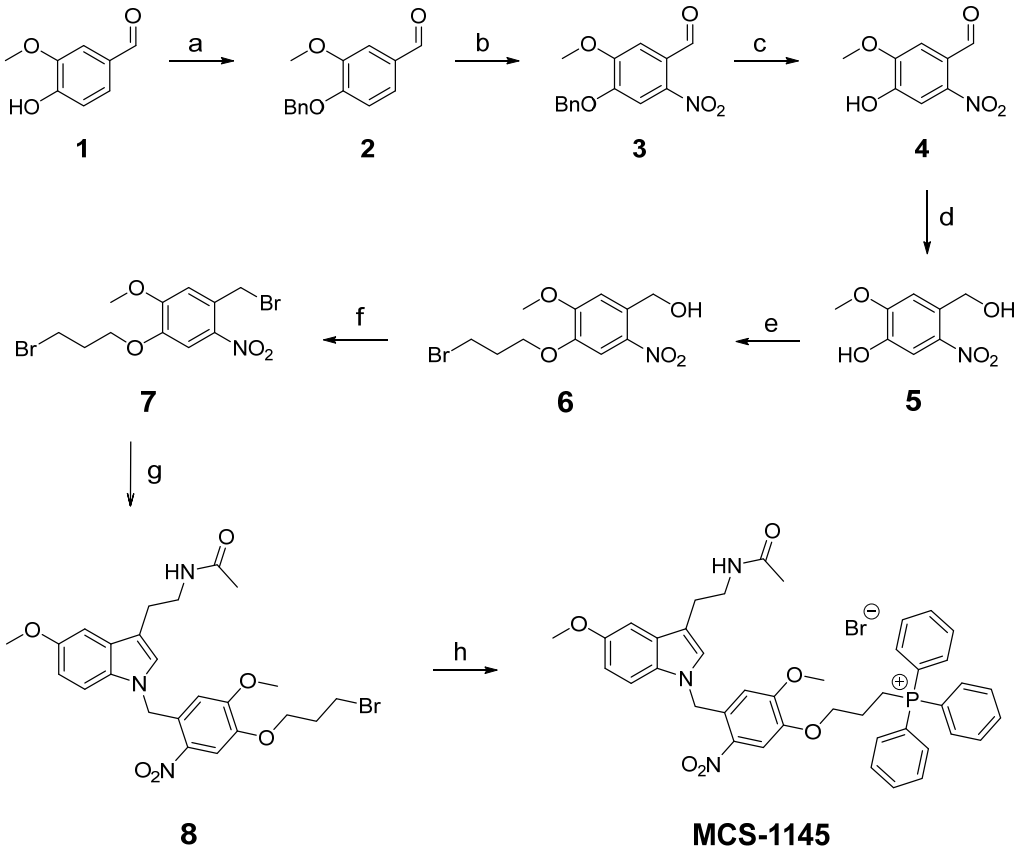

Figure 2. Synthesis of compound **MCS-1145**. Reagents and conditions: **(a)** i) K_2CO_3, DMF, RT, 1h; ii) BnBr, RT to 85 °C, 3 days, 62%; **(b)** HNO_3 65%, CH_3COOH, RT, 4 days, 51%; **(c)** TFA, RT, 4 days, 71%; **(d)** $NaBH_3$, EtOH, RT, ON, 95%; **(e)** K_2CO_3, 1,3-dibromopropane, Acetone, EtOH, RT to reflux,

ON, 70%; **(f)** PBr_3, DCM, RT, ON, 58%; **(g)** i) Melatonin, NaH, DMF, RT, 1.5 h; ii) Compound **7**, DMF, -55 °C to 5 °C, 4 h, 9%; **(h)** TPP, ACN, RT to reflux, 2 days, 75%. **MCS-0382** was synthesized as previously described (Somalo-Barranco et al., 2022). See also **Figure S1** for details on the synthesis of **MCS-1144**, the acetate-derivative of the nitrobenzyl-TPP^+ caging group present in MCS-1145.

In addition to melatonin, the photolysis of **MCS-1145** will result in some other products coming from the nitrobenzyl-TPP^+ caging group present in this molecule. Therefore, we planned to assess the possible effect of these photoproducts towards melatonin receptors. In order to test the effect of these molecules independently of melatonin, **MCS-1144**, an acetate derivative of the nitrobenzyl-TPP^+ caging group present in MCS-1145, was synthesized. Details on the synthesis of **MCS-1144** are provided in the SI (**Figure S1**). Caged compound **MCS-1144** would release receptor inactive acetate upon illumination, serving as a control of the molecules obtained by photolysis.

Photochemical properties of MCS-1145.

UV-Vis absorption spectrum was recorded for **MCS-1145**, in order to determine the wavelengths that are suitable for the photolytic reaction. The compound showed two absorption maxima at λ = 304 nm and λ = 346 nm (**Figure 3A**), very similar to the UV-Vis profile of **MCS-0382** (**Figure 3B**). These wavelengths indicated that the uncaging reaction should be performed with light of wavelengths ranging from 300 to 400 nm, typical for DMNB derivatives. In agreement with the photochemical characterization of the previously described **MCS-0382**, we used the same light source to perform the uncaging experiments for **MCS-1145**.

Therefore, we used a laser with a wavelength in the visible spectrum range (λ= 405 nm, 2.37 mW/mm^2) to trigger photolysis, in order to avoid the cell damage associated to UV light. Aqueous solutions of **MCS-1145** were illuminated for different periods of time (t = 0, 3, 5, 8, 10, 15 and 30 min) and subsequently analyzed by HPLC-MS. For each time point, the amount of released melatonin was quantified, as well as the remaining concentration of caged

compound. Importantly, the photolysis of **MCS-1145** also revealed the formation of N^1-acetyl-N^2-formyl-5-methoxykynuramine (AFMK), detected during the uncaging of the previously reported caged melatonin ligands (**Figure S2A**) (Somalo-Barranco et al., 2022). AFMK is the main product of the oxidative metabolism of melatonin in the brain (Galano et al., 2013; Tan et al., 2007). Its formation is favored by the presence of oxygen and light and it involves a pyrrole-ring cleavage of melatonin (Bonnefont-Rousselot et al., 2011; Hevia et al., 2014). Therefore, the concentration of AFMK was systematically monitored in our assays. Concentrations of the other species in solution were calculated with the equation extracted from their calibration curves (**Figure S2B-F**).

MCS-1145 presented a similar uncaging rate to that of **MCS-0382**, with the maximal amount of released melatonin reached after 10 minutes of light application and a total disappearance of **MCS-1145** after 15 minutes (**Figures 3C-D**, green and blue lines). For **MCS-1145**, an uncaging efficiency of 55% was determined, value that was slightly higher for **MCS-0382**, with a 65% uncaging efficiency. In both cases, quantification of AFMK revealed a minor formation of this photolytic product under our assay conditions, especially for **MCS-1145** (**Figures 3C-D**, grey lines). Slight degradation was detected for **MCS-0382** and **MCS-1145**, mainly due to the formation of short-lived intermediates upon photolysis of *o*NB-derivatives (Kohl-Landgraf et al., 2014). The formation of these unknown by-products was not quantified.

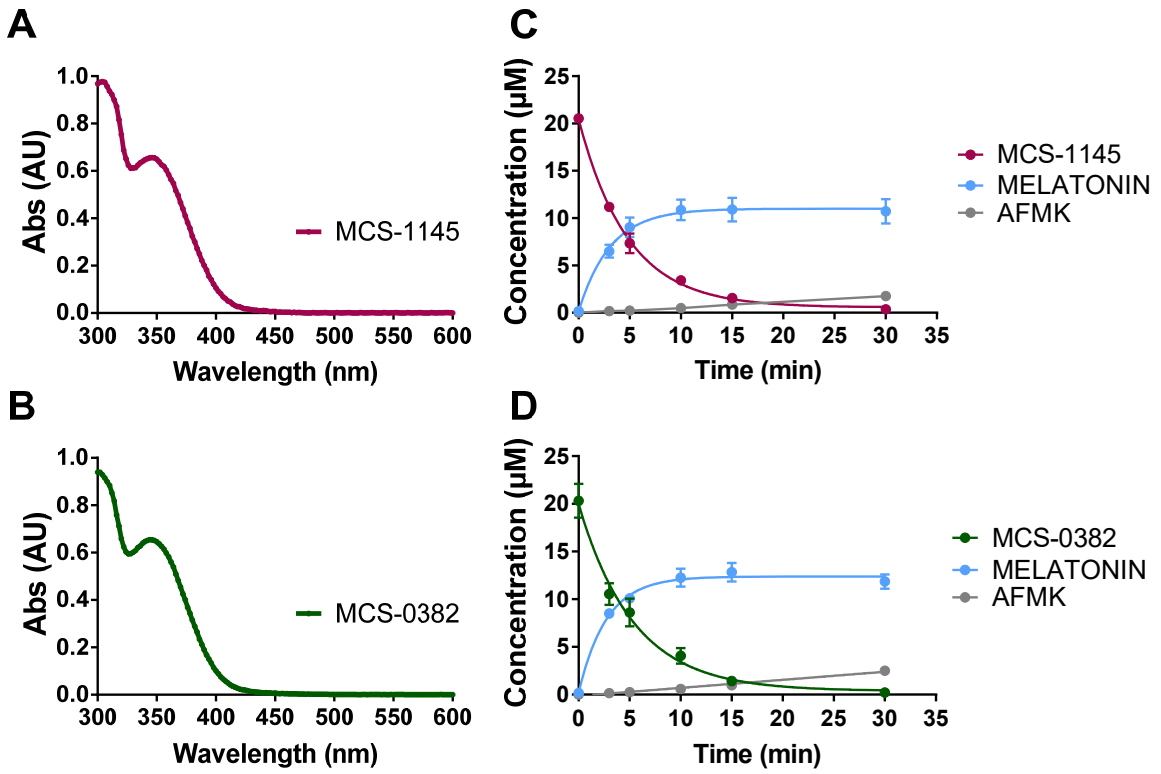

Figure 3. Photochemical characterization of compounds **MCS-1145** and **MCS-0382**. UV-Vis absorption spectra of **MCS-1145 (A)** and **MCS-0382 (B)**. Photolysis of compounds **MCS-1145 (C)** and **MCS-0382 (D)** at λ = 405 nm in a 20 µM aqueous solution (PBS/DMSO, 98:2). Concentrations of the species were calculated from the calibration curves of melatonin, AFMK and the compounds, obtained by HPLC-MS analysis. Data are expressed as mean ± SEM of three independent experiments. See also **Figure S2** for further data on the photochemical characterization of the compounds.

Affinity of MCS-1145 for MT_1 and MT_2 receptors under dark and light conditions

The affinity of **MCS-1145** for melatonin receptors was determined in dark conditions and after light application in competition binding assays with 2-[^{125}I]iodomelatonin (2-[^{125}I]-MLT). These experiments were performed in crude membranes from HEK293 cells stably expressing human MT_1 or MT_2 receptors. The reference compound, melatonin, bound both receptors with high affinity, displaying similar sub-nanomolar affinity for MT_1 and MT_2 (**Table 1**). In dark conditions, **MCS-1145** displayed modest affinity for both the receptors, validating the chemical design of the caged compound (**Table 1**). The affinities were in the high micromolar range, 100- (MT_2) to 1000- (MT_1) fold lower than melatonin and similar to the affinity of the non-mitochondria-targeted **MCS-0382** (**Figures 4, Table 1**). The slightly higher affinity for MT_2 is in

agreement with the larger binding site of this receptor subtype, as it accommodates bulky substituents at the *N1* or C2 positions of melatonin in the hydrophobic subpocket of MT_2 (Johansson et al., 2019).

Table 1. Affinity and agonist potency of **MCS-1145** and **MCS-0382** in HEK293 cells expressing MT_1 or MT_2 receptors.

	2-[^{125}I]-MLT competition		**cAMP inhibition**	
	pK_i ± S.E.M.		**pEC_{50} ± S.E.M.**	
Ligand	MT_1	MT_2	MT_1	MT_2
Melatonin	9.52 ± 0.24	9.84 ± 0.30	9.87 ± 0.25	9.95 ± 0.16
MCS-0382	6.32 ± 0.23[a]	6.56 ± 0.19 [a]	6.75 ± 0.24 [a]	8.03 ± 0.30 [a,b]
MCS-0382+Light	8.90 ± 0.22 [a]	9.16 ± 0.23 [a]	9.59 ± 0.15 [a]	9.48 ± 0.24 [a]
MCS-1145	6.70 ± 0.48	7.39 ± 0.27	6.93 ± 0.26	7.15 ± 0.31
MCS-1145+Light	8.88 ± 0.44	9.55 ± 0.07	9.47 ± 0.29	9.36 ± 0.24

The affinity was measured in 2-[^{125}I]-MLT competition experiments and is expressed as mean pK_i ± S.E.M. Agonist potency was measured as inhibition of forskolin-stimulated cAMP production and is expressed as pEC_{50} ± S.E.M. (M). Data correspond to the mean of at least three independent experiments, each of them performed using at least eight different ligand concentrations. **[a]** data taken from *Somalo-Barranco et al., 2022.* **[b]** All compounds were full agonists with the exception of compound MCS-0382, acting as a partial agonist on MT_2, with a maximal efficacy (E_{max}) equal to 38.8 ± 5.4, expressed as a percentage of the maximal effect observed with melatonin (=100%).

Upon illumination at 405 nm, **MCS-1145** showed an increase in apparent affinity on both receptors with pK_i values close to melatonin and light-activated **MCS-0382** (**Figures 4, Table 1**). These results confirm the light-mediated generation of biologically active melatonin and are in agreement with the relatively high uncaging efficiency of **MCS-1145**.

In control experiments, we made sure that light exposure had no significant effect on the pK_i of melatonin (**Figures S3, Table S1**). Consistently, the impact of AFMK, the main degradation

product generated at 8% upon illumination of melatonin (**Figure S2A**), could be also excluded due to its low affinity ($pK_i \approx 5$) for melatonin receptors (**Figure S3, Table S1**). We also excluded an effect of the caging group (compound **MCS-1144**) on melatonin binding to MT_1 and MT_2 by determining the pK_i of melatonin in the presence of equimolar amounts of **MCS-1144** (**Figure S4, Table S1**). Consistently **MCS-1144** alone showed 1000-fold lower affinity for MT_1 and MT_2 than melatonin, which was not changed by pre-illumination at 405 nm (**Figure S4, Table S1**). Taken together, these results indicate that the caging group of **MCS-1145** and its photolytic side products showed no impact on the pharmacological properties of uncaged melatonin.

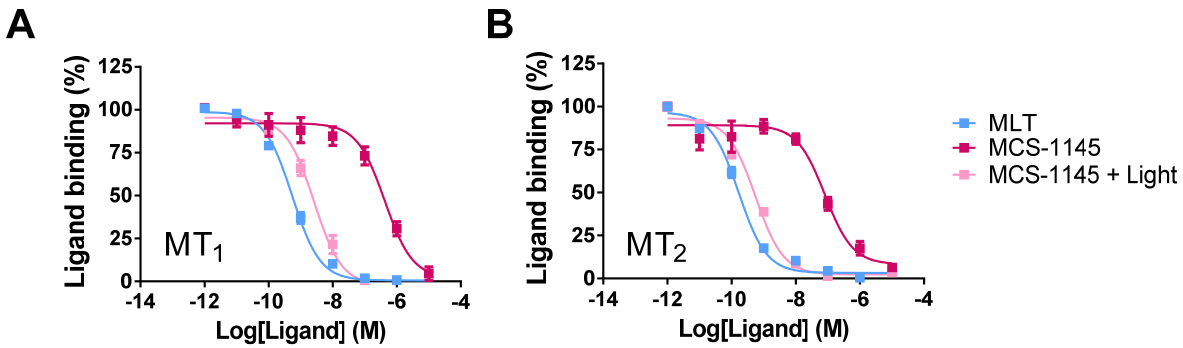

Figure 4. Competition of 2-[^{125}I]-MLT binding by melatonin and **MCS-1145** before and after light exposure, in crude membranes from HEK293 cells stably expressing MT_1 or MT_2 receptors. Light is applied to the ligands for 10 minutes prior to incubation with the membranes, using the laser as a light source (405 nm, 2.37 mW/mm^2). Data are expressed as mean ± SEM from 4 to 5 independent experiments (**A**. Melatonin n = 5, MCS-1145 (Dark) n = 5, MCS-1145 (Light) n = 4; **B.** Melatonin n = 5, MCS-1145 (Dark) n = 5, MCS-1145 (Light) n = 4). Data are represented as percentage of maximal binding in the absence of compounds.

Signaling properties of MCS-1145 on MT_1 and MT_2 receptors under dark and light conditions

The best-characterized signaling pathway for melatonin receptors is the inhibition of cAMP production via coupling to $G_{i/o}$ proteins. The capacity of **MCS-1145** to inhibit forskolin-stimulated cAMP production was assessed in HEK293 cells stably expressing MT_1 or MT_2 receptors. Melatonin was used as a standard and inhibited forskolin-stimulated cAMP production as expected, with pEC_{50} values in the sub-nanomolar concentration range (**Figure**

5, Table 1). Prior to light activation, **MCS-1145** behaved as a full agonist for both MT_1 and MT_2, displaying lower pEC_{50} values (≈7) in comparison to melatonin (**Table 1**). Upon uncaging, the compound reached an apparent EC_{50} value similar to melatonin and the light-activated **MCS-0382** for MT_1 and MT_2 (**Table 1**), validating the efficient generation of biologically active melatonin after light activation.

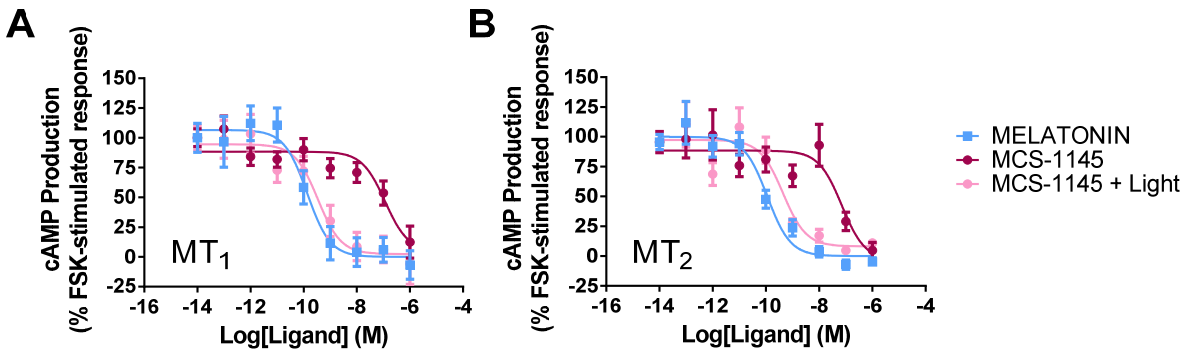

Figure 5. Inhibition of cAMP production by melatonin and **MCS-1145** before and after light exposure in cells stably expressing MT_1 (**A**) and MT_2 (**B**). Light is applied to the ligands for 10 minutes prior to incubation with the cells, using the laser as a light source (405 nm, 2.37 mW/mm^2). Data are expressed as mean ± SEM from 5 to 8 independent experiments (**A.** Melatonin, MCS-1145 (Dark), MCS-1145 (Light) n = 6; **B.** Melatonin n = 8, MCS-1145 (Dark) n = 6, MCS-1145 (Light) n = 5). Data are presented as percentage of forskolin-stimulated response and normalized to the maximal and minimal melatonin effect. The amplitude of cAMP inhibition before normalization varied between 50 and 75%.

Mitochondrial localization of MCS-1145

In order to measure the signaling properties of **MCS-1145** in real-time, we used a bioluminescence resonance energy transfer (BRET)-based cAMP sensor, the so-called CAMYEL (*cAMP* sensor using *Y*FP-*E*pac-R*L*uc) sensor (**Figure 6A**) (Jiang et al., 2007). Binding of cAMP to the sensor results in a decrease of BRET signal as the energy donor and acceptor are moving apart. In this assay, we used the property of melatonin to induce a strong change in BRET signal (≈200 mBu) with sub-nanomolar potency (pEC_{50} = 9.40 ± 0.14) by potentiating the forskolin response at high MT_1 expression levels (**Figure S5A,B**). Consistent with results obtained in the cAMP accumulation assay, the caged form of **MCS-1145** (dark condition) behaved as a full agonist with micromolar potency (pEC_{50} = 6.09 ± 0.11) (**Figures 6B, S5C**). We then induced uncaging with a short (20 s) light pulse to induce a partial but

significant release of melatonin illustrated by the left-shifted apparent pEC_{50} of 7.22 ± 0.09 of **MCS-1145** under these conditions (**Figure 6B, S5D,E,F**). Longer illumination times impacted on the stability of the highly photosensitive Rluc substrate coelenterazine-h (**Figure S8**). At 100 nM of **MCS-1145**, the responses of the caged and uncaged forms could be perfectly separated as the caged form (dark condition) showed no response and the uncaged from (light condition) displayed a clear response with a maximal amplitude close to that of the melatonin reference (**Figure 6C**). This behavior was not due to the mitochondria-targeting of **MCS-1145** as similar observations were made for **MCS-0382** with pEC_{50} values of 5.78 ± 0.19 and 7.47 ± 0.14 under dark and light conditions, respectively (**Figure S7A-C**).

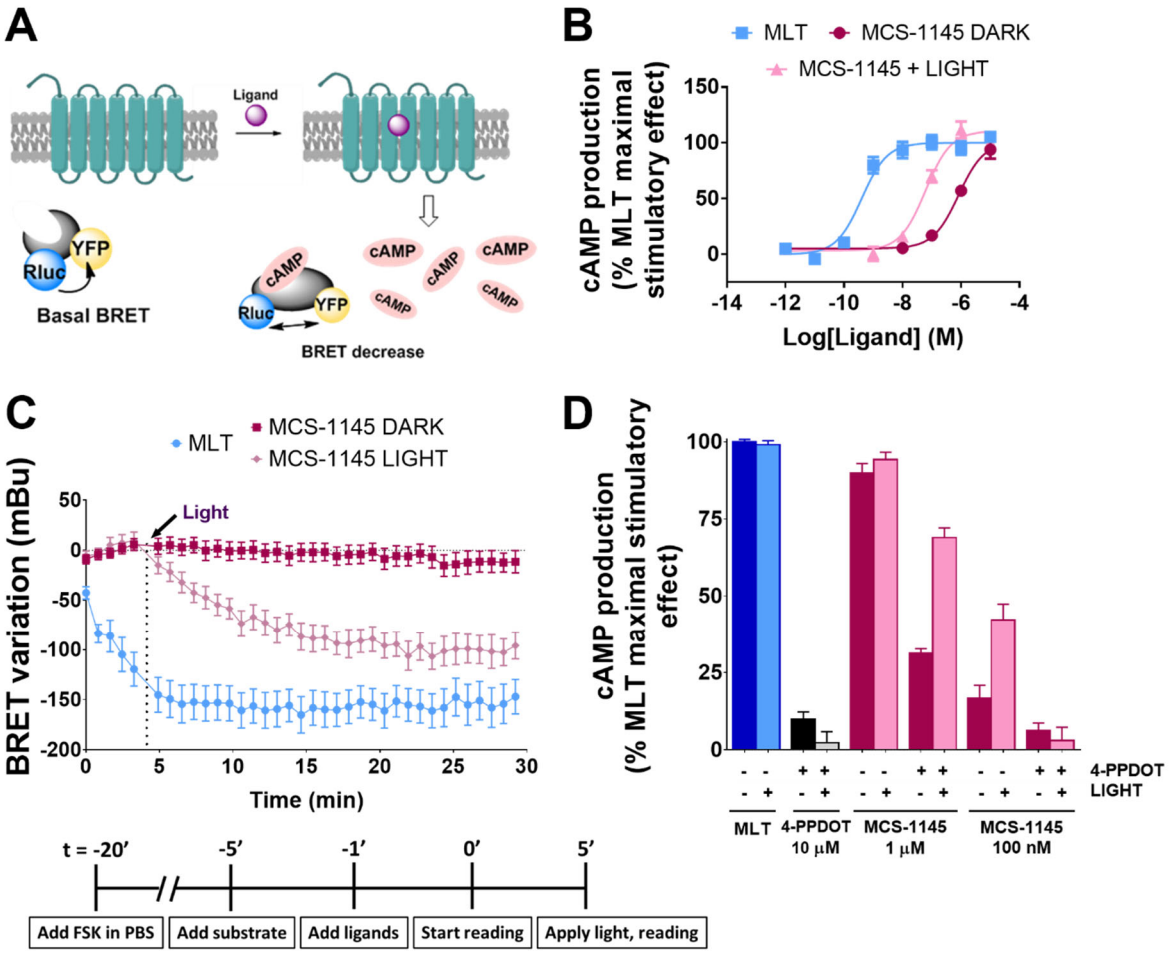

Figure 6. Activity of **MCS-1145** monitored with real-time cAMP sensor. **(A)** Schematic representation of the Epac-based CAMYEL sensor, adapted from Ayoub et al. (Ayoub et al., 2015). **(B)** cAMP production by melatonin and MCS-1145 in the absence and in the presence of light. Concentration-response curves for melatonin and MCS-1145 were generated from the time-course assays at 15

minutes. Data were expressed as mean ± SEM of 3 independent experiments and normalized to forskolin alone (0%) and the melatonin maximal stimulatory effect (100%). **(C)** Time-course of BRET variation induced by melatonin and MCS-1145, in the presence and in the absence of light (both at 100 nM). Data were expressed as mean ± SEM of 6 independent experiments. **(D)** Control of MCS-1145 activity with the presence of 4P-PDOT at 10 µM. Data were generated from the time-course BRET assays at 15 minutes. Data were expressed as mean ± SEM of 3 independent experiments and normalized to melatonin maximal stimulatory effect at 100 nM (= 100%). In all cases, light was applied to the cells for 20 s, using the laser as a light source (405 nm, 2.37 mW/mm^2). See also **Figures S5**, **S6** and **S7**.

We then determined the activity of **MCS-1145** in the presence of a saturating concentration of the melatonin receptor antagonist 4P-PDOT (10 µM) for MT_1 (**Figure 6D**). 4P-PDOT alone had no effect as expected. At a high concentration, **MCS-1145** (1 µM) was similarly active than the melatonin reference in its caged (dark) and uncaged (light) form. The presence of 4P-PDOT largely reduced the **MCS-1145** signal under dark conditions whereas light application reverted this loss of activity, thereby demonstrating the efficient release of high affinity melatonin upon uncaging and the subsequent displacement of the antagonist. At 100 nM, **MCS-1145** was inactive under dark conditions but become partially active upon light application consistent with melatonin photorelease. At this concentration the effect was fully blocked by 4P-PDOT. In conclusion, the pharmacological behavior of 4P-PDOT in our system is perfectly compatible with the generation of melatonin from **MCS-1145** upon light activation.

We then compared the response of the mitochondria-targeted **MCS-1145** with that of the untargeted **MCS-0382** at 100 nM in cells expressing MT_1 and CAMYEL (**Figure 7A**). Light application promoted a fast decrease of the BRET signal with identical rates and maximal levels that were comparable to that of melatonin at the same concentration. This indicates that **MCS-1145** and **MCS-0382** have similar uncaging efficiencies generating similar amounts of melatonin.

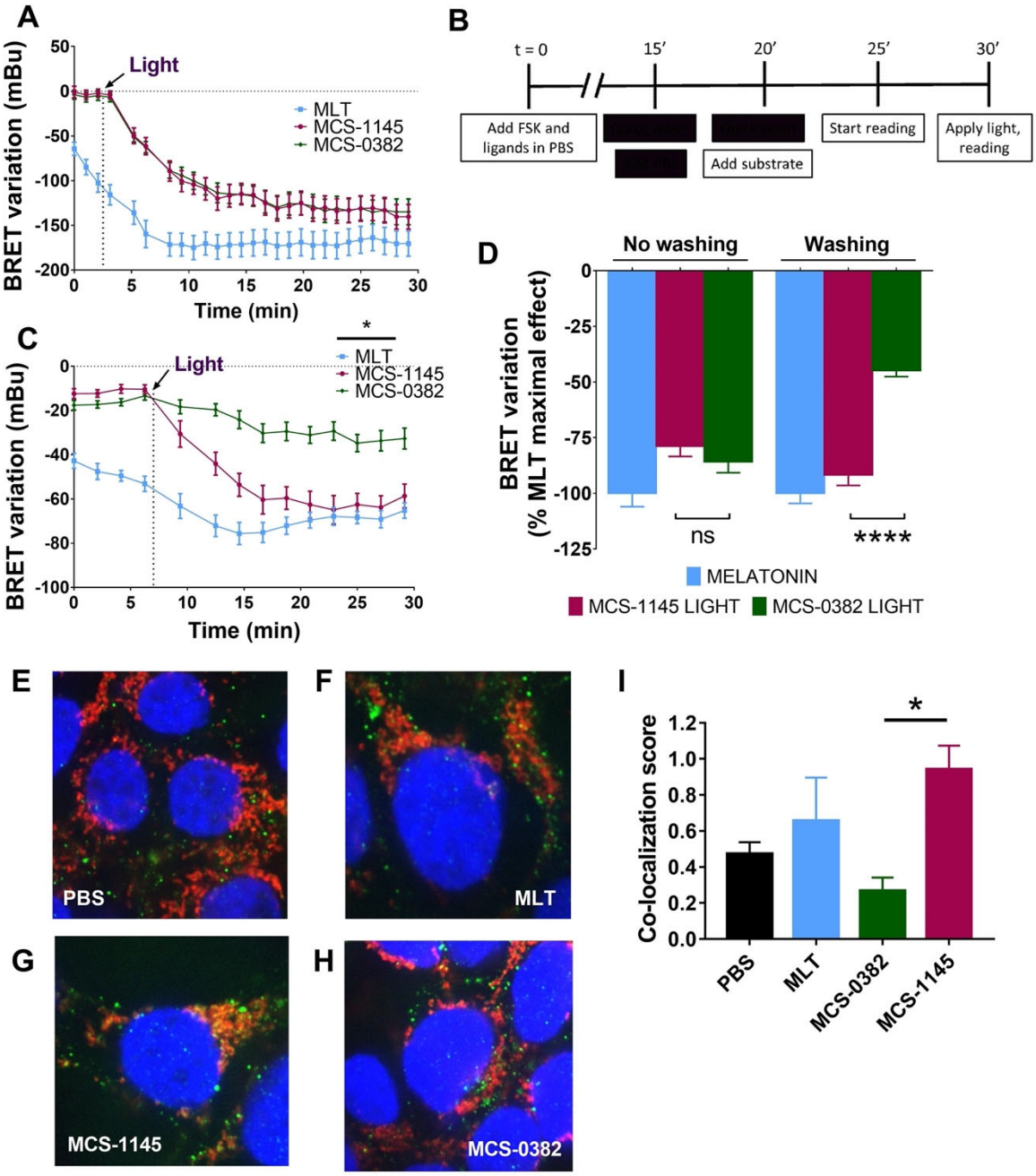

Figure 7. Different responses of **MCS-1145** versus **MCS-0382** determined by the BRET-based CAMYEL sensor on MT_1. **(A)** BRET variation mediated by melatonin and compounds MCS-0382 and MCS-1145 following the standard protocol (absence of washing). All compounds are tested at 100 nM. **(B)** Experimental protocol for light-activated compounds, including washing steps. **(C)** BRET variation mediated by melatonin, MCS-0382 or MCS-01145 (100 nM each) in the presence of FSK following the washing protocol. **(D)** Quantification of BRET variation at 15 min mediated by MCS-0382 and MCS-01145 after light exposure in the different protocols. Data are presented as percentage of melatonin maximal effect for each condition. Statistical analysis is performed by Student's *t*-test, where ns: not significant and ****: $p < 0.0001$. Data shown in panels **A,C,D** are expressed as mean ± SEM from 6 independent experiments. Light was applied to the cells for 20 s, using the laser as a light source (405 nm, 2.37 mW/mm^2). **(E-H)** Representative immunofluorescence images of HEK293T cells previously incubated for 15 minutes with PBS **(E)**, melatonin **(F)**, MCS-1145 **(G)** or MCS-0382 **(H)**, all them at 100 nM. DAPI (blue), anti-TOMM20 (red) and anti-melatonin (green) antibody staining. **(I)** Co-localization analysis (Manders' colocalization coefficient) of the fractional overlap between the staining of the anti-melatonin antibody and the staining of the TOMM20 antibody. Quantification is performed to the full

image (average number of cells analyzed per condition: PBS 16±5; melatonin 15±4; MCS-1145 15±3; MCS-0382 16±3. Data are expressed as mean ± SEM of three independent images. Statistical analysis is performed by Student's *t*-test, where *p<0.05.

To demonstrate the enrichment of **MCS-1145** inside the cell compared to the untargeted **MCS-0382**, we included two washing steps 15 minutes after addition of the compounds at 100 nM (**Figure 7B**) in the signaling experiment with the real-time cAMP sensor. Under dark conditions, neither **MCS-0382** nor **MCS-1145** had any effect and only the reference forskolin signal was detected (**Figure 7C**). The reference agonist melatonin showed approximately 40% remaining activity compared to the protocol without washing steps (compare panel A and C). Application of light induced a fast decrease of the BRET signal for **MCS-1145** upon uncaging, reaching a similar response to that of melatonin (**Figures 7C,D**). In contrast, **MCS-0382** only induced a partial change of the BRET signal after light application (**Figures 7C,D**). This indicates that untargeted **MCS-0382** is easily washed out whereas **MCS-1145** is retained and releases significant amounts of melatonin upon light-induced uncaging. These data are in agreement with the random distribution of **MCS-0382** throughout the cell and mitochondrial retention of **MCS-1145**.

Accumulation of uncaged **MCS-1145** specifically in mitochondria was supported by immunofluorescence microscopy experiments. Wild-type HEK293T cells were pre-incubated with compounds (100 nM), washed twice before fixation and incubated with antibodies recognizing the mitochondrial marker protein TOMM20 (red) and with anti-melatonin antibodies (green) recognizing melatonin and the melatonin moiety of **MCS-0382** and **MCS-1145** (Chen et al., 2020a; Wang et al., 2020) (**Figure 7E-H**). The co-localization was quantified by using Manders' coefficient, which is the degree of overlap between two channels. In the absence of compounds only background staining was observed with the anti-melatonin antibody that partially colocalize with the TOMM20 staining (Manders' Coefficient score of 0.50) (**Figure 7E,I**). Similarly, only background signals were observed for the melatonin and the **MCS-0382** condition (Manders' Coefficient score of 0.30-0.65) (**Figure 7F,H,I**) and substantial co-localization for the **MCS-1145** condition (Manders' Coefficient score of 0.95)

(**Figure 7G,I**) suggesting the accumulation of **MCS-1145** in mitochondria whereas **MCS-0382** and melatonin are rapidly washed out.

To provide further evidence for the mitochondrial enrichment of **MCS-1145**, we detected compounds **MCS-382** and **MCS-1145** by HPLC-MS in mitochondria isolated from cells treated with either compound (5 µM, 30 min) (**Tables S2 and S3**). While **MCS-0382** was detectable at 19 nM, a concentration close to the limit of quantification (11 nM), **MCS-1145** was readily detectable at a concentration that was at least 26 times higher (492 nM) ($P < 0.001$). This result indicates that the addition of the TPP group in **MCS-1145** promotes a pronounced increase of mitochondrial accumulation of the compound as expected.

Collectively, cAMP, immunofluorescence and HPLC-MS data support the specific mitochondrial accumulation of caged **MCS-1145** as compared to **MCS-0382** and melatonin.

Mitochondrial b-arrestin2 recruitment to MT1 by melatonin and MCS-1145.

Recruitment of β-arrestin is a general property of GPCRs including the MT1 receptors (Ref). The presence of β-arrestin in mitochondria raises the possibility that this can also occur in mitochondria (Suofu). To monitor beta-arrestin recruitment in a subcellular compartment-specific manner, we designed a split-NanoBiT assay that is based on the complementation of two fragments of the Nanoluciferase (Nluc), HiBiT and LgBiT (Lg). The HiBit fragment is fused to the C-terminus of MT_1 and the LgBiT fragment to a localization sequence for subcellular compartments (OMM, IMS, plasma membrane (PM)). Nluc complementation occurs only when HiBiT and Lg are located in the same compartment generating a sub-compartment-specific energy donor to monitor recruitment of ß-arrestin2 fused to the yellow fluorescent protein (YFP) energy donor by BRET. To validate this assay format, we first monitored ß-arrestin2 recruitment to MT_1 at the plasma membrane using the well-known GAP43-based localization sequence (Ref??) to generate the PM-Lg localization sensor. Melatonin addition induced the expected rapid increase in BRET signal reaching its maximum within 10 minutes. A similar

melatonin-induced BRET was observed with the IMS-Lg sensor but not with the OMM-Lg sensor further confirming the specificity of the IMS sensor signal. The proper localization of the OMM-Lg and IMS-Lg sensors was confirmed by immunofluorescence microcopy and co-colcalization with the TOMM20 (Fig. X). These data support additional support for the functional expression of MT1 in the OMM.

Inhibition of mitochondrial respiration by melatonin and MCS-1145.

Mitochondrial respiration is one of the mitochondrial core functions but the effect of mitochondrial MT_1 on this function is unknown. To address this question, we measured the oxygen consumption rate of mitochondria isolated from HEK293 cells and mouse cerebellum. Addition of melatonin (1 µM) diminished oxygen consumption by 20% in mitochondria isolated from MT_1 expressing HEK293 cells but not in control cells expressing the green fluorescent protein (GFP) or in cells expressing MT_2 (**Figure 8A**). A similar effect was observed in mitochondria isolated from the cerebellum of wild-type C57bl/6 mice known to express melatonin receptors (Mazzucchelli et al., 1996) (**Figure 8B**). Importantly, this effect was not observed in mitochondria isolated from MT_1-KO mice but recapitulated in mitochondria isolated from MT_2-KO mice (**Figure 8B**). This result indicates that melatonin inhibits mitochondrial respiration by specifically acting on mitochondrial MT_1 receptors.

Consistently with the liberation of biologically active melatonin upon light activation, uncaged **MCS-1145** and **MCS-0382** inhibited the oxygen consumption rate of mitochondria from MT_1 expressing HEK293 cells but not in control cells (**Figure 8C**). This effect was dependent on light exposure of the compounds as they were inactive in their caged state (dark condition) (**Figure 8D**). These data show that melatonin generated through uncaging of **MCS-1145** and **MCS-0382** inhibit mitochondrial respiration similar to exogenous melatonin. We then wanted to discriminate the effects of the mitochondria-targeted **MCS-1145** and the untargeted **MCS-0382** on mitochondrial respiration by pre-incubating intact MT_1-expressing HEK293 cells with the caged ligands prior to mitochondria isolation. Light was then applied to isolated

mitochondria and the oxygen consumption rate measured. Consistent with the mitochondria targeting of **MCS-1145**, light had a stronger effect on the oxygen consumption rate than on the non-targeted **MCS-0382** (**Figure 8E**). Similar results were obtained when the activity of **MCS-1145** and **MCS-0382** after light application was compared to the activity of the compound under dark conditions (**Figure 8F**). While the uncaged state of **MCS-1145** showed a clear effect on the oxygen consumption rate in comparison with its caged state, **MCS-0382** was ineffective in this assay format.

Overall, these results confirm that **MCS-1145** accumulates in mitochondria where it liberates melatonin to inhibit mitochondrial respiration through MT_1 receptors.

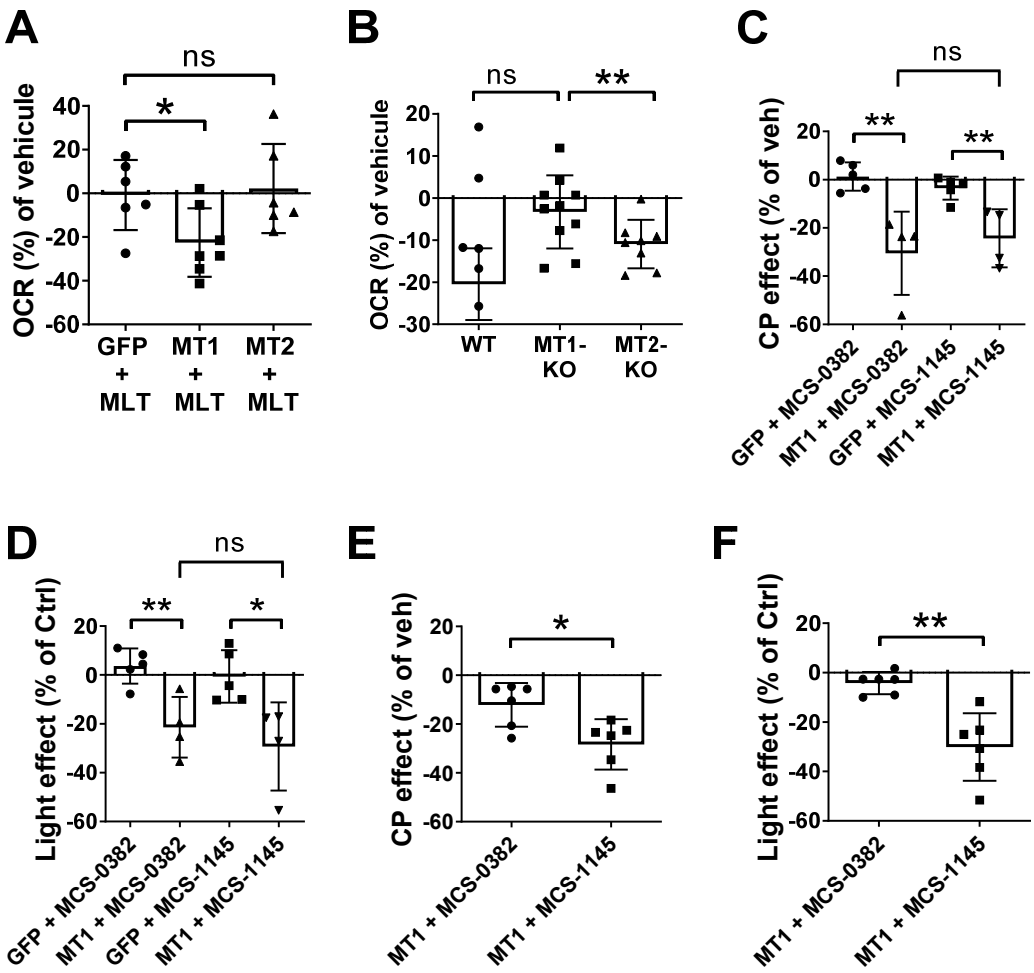

Figure 8. Effect of melatonin, **MCS-1145** and **MCS-0382** on mitochondrial respiration. **(A)** Effect of melatonin (1 µM) on the oxygen consumption rate (OCR) of isolated mitochondria from HEK293 cells expressing MT_1, MT_2 or GFP (control). **(B)** Effect of melatonin (1 µM) on mitochondria isolated from cerebellum mouse brain lysates from wild-type, MT_1-KO or MT_2-KO mice. **(C)** Effect of uncaged MCS-1145 and MCS-0382 (5µM each) vs. vehicles and **(D)** caged (dark condition) vs. uncaged (light

condition) MCS-1145 and MCS-0382 on the oxygen consumption rate (OCR) of isolated mitochondria from HEK293 cells expressing MT_1 or GFP (control). **(E)** Effect of the MCS-1145 and MCS-0382 (5µM each) vs. vehicles, when added to intact MT_1-expressing HEK293 cells followed by mitochondria isolation. **(F)** Effect of the light on the respiration by comparing the caged (dark condition) vs. uncaged (light condition), in mitochondria isolated from MT_1-expressing HEK293 cells and pre-incubated with ligands. (E,F) Isolated mitochondria were illuminated directly in the measuring cuvette with a laser as the light source (5 minutes, 405 nm, 2.37 mW/mm^2) prior to measuring oxygen consumption rate. Control conditions (vehicle or dark condition) were run in parallel in a second cuvette. Data are expressed as mean ± SEM from 3 independent experiments and presented as a percentage of the control condition. Statistical analysis is performed by the unpaired two-tailed *t*-test, where ns: not significant, *: $p < 0.05$ and **: $p < 0.01$. CP, compound.

Discussion

Using molecules whose activity can be controlled by light is a promising approach to modulate biological processes with high precision, low toxicity and safety. Photoactivation has been already proposed to generate tools for the control of melatonin receptors activation, in order to contribute to a better understanding of receptor-induced signaling and function (Somalo-Barranco et al., 2022). In this context, light-activable molecules might be of particular interest to study the role of the previously described mitochondrial MT_1 receptors (Gbahou et al., 2017; Suofu et al., 2017). Caged compounds promote an abrupt change of the concentration of the active molecule in the action site, thus providing a high spatiotemporal control of the process (Hansen et al., 2015). Nevertheless, caged compounds are generally distributed all over the cell, which hinders the specific activation or control of the events that occur at an intracellular level.

To address this limitation, we present here the synthesis and the functional validation of a mitochondria-targeted caged compound for melatonin receptors, **MCS-1145**. Following the caging strategy that was employed for the development of the first family of caged melatonin ligands, **MCS-1145** was designed. Therefore, a DMNB-based photocleavable group was attached at the *N1*-position of melatonin. This caging group incorporated a hydrophobic and positively charged TPP^+ moiety to favor mitochondrial accumulation of the compound. The presence of a relatively bulky group at the *N1*-position of melatonin promoted an expected loss

of binding affinity for both MT_1 and MT_2, without displaying receptor-subtype selectivity (Journé et al., 2014; Lira-Rocha et al., 2002; Viault et al., 2016). **MCS-1145** displayed a good uncaging efficiency, confirmed by its excellent apparent pK_i and EC_{50} values on binding affinity and inhibition of cAMP production after light application. Time-resolved cAMP assays allowed us to provide experimental evidence for the intracellular retention of the mitochondria-targeting **MCS-1145**. Interestingly, the inclusion of a washing step after pre-incubation of the cells with ligand abolished the effect of non-targeted **MCS-0382** on MT_1 activation, while the effect of the mitochondria-targeted **MCS-1145** was maintained. Co-localization of **MCS-1145** but not **MCS-0382** with the mitochondrial marker TOMM20 is fully compatible with the retention of **MCS-1145** in mitochondria. Light-mediated generation of melatonin as well as exogenous melatonin inhibited respiration in isolated mitochondria from cells expressing MT_1, which further supports the functional relevance of melatonin receptors in the mitochondria. Furthermore, the presence of the compounds during mitochondria isolation suppressed the effect of non-targeted **MCS-0382** on the oxygen consumption rate in mitochondria isolated from MT_1-expressing cells, while the effect of the mitochondria-targeted **MCS-1145** was maintained. This seems to be a specific property of MT_1 receptors as no effect was observed with mitochondria isolated from MT_2-expressing cells. In light of the numerous receptor-independent effects attributed to melatonin in mitochondria (Reiter et al., 2018), it was also important to show that the inhibitory effect on respiration was not visible in mitochondria devoid of MT_1 receptor expression.

Emerging intracellular GPCRs are transforming the conception about GPCR signaling and regulation (Vilardaga et al., 2014). Many examples have been reported, including the cannabinoid receptor type 1 in mitochondria or the endosomal parathyroid hormone receptor type 1 (PTHR). Many aspects of the mechanism of signal transduction of these receptors upon ligand binding remain elusive. In general terms, two mechanisms have been reported to explain intracellular signaling for GPCRs (Wang et al., 2018). First evidences about intracellular GPCRs revealed that they are able to mediate signaling inside the cell only after receptor internalization, process that occur to avoid receptor desensitization and terminate

signaling (Chuang and Costa, 1979; Wang et al., 2018). Furthermore, it was discovered later that GPCR signaling could be also promoted by the activation of receptors that are already located in different subcellular compartments. Of interest, the activation of differently-located receptors can induce distinctive responses (Tadevosyan et al., 2016), which can be crucial to decipher the implications of GPCRs at a physiological level, as it is the case of intracellular melatonin receptors. More precisely, the development of the first cell-impermeable agonist for melatonin receptors allowed the distinction between G_i/cAMP signaling from the MT_1 receptor at the cell surface and the signaling from MT_1 receptors at the mitochondria. The presence of MT_1 in neuronal mitochondria was reported for the first time in 2011 (Wang et al., 2011), and the authors also suggested the neuroprotective role of melatonin upon specific activation of intracellular receptors. In fact, they observed that depletion of mitochondrial MT_1 increased neuronal death, thus accelerating neurodegenerative processes. These evidences were further confirmed by Suofu et al., 2017, whose work showed that overexpression of mitochondrial MT_1 receptor reduced caspase-3 activation and blocked stress-mediated release of cytochrome *c* after activation with melatonin. The authors also demonstrated the contribution of intracellular MT_1 on preventing neuronal death on cerebral ischemic injury *in vivo*. Similar results were obtained by Zhang et al., 2013, in which melatonin exerted neuroprotective effects in transgenic amyotrophic lateral sclerosis mice through the activation of MT_1 receptors. Moreover, other studies reveal the important role of melatonin in mitochondrial physiology, by preventing mitochondrial damage produced by ischemia or hypoxia (Huang et al., 2013; Yang et al., 2013). Mitochondria are frequently described as the powerhouse of the cell, and dysfunctions are related with the onset of neurological disorders (Lin and Beal, 2006). Therefore, there is evidence suggesting the role of melatonin in neurodegenerative disorders, such as Alzheimer's or Huntington's diseases (Wongprayoon and Govitrapong, 2017). In fact, low levels of melatonin and a reduced expression of MT_1 – more precisely, mitochondrial MT_1, were systematically detected in different neurodegenerative diseases (Kalliolia et al., 2014; Liu et al., 1999; Zhang et al., 2013). Taken

together, these results suggest that protective effects of melatonin can, at least in part, be mediated and dependent of MT_1 activation in the mitochondria, thus confirming the existence of an intracellular signaling pathway for melatonin receptors.

Furthermore, the attachment of fluorescence caging groups could be another aspect to consider, as it would allow its quantification in the cell and to monitor the subcellular localization of the probe (Farley et al., 2021). Examples of these groups would be BODIPY- or coumarin-based photo-protecting groups. The presence of organelle-targeting moieties and the light-controlled activity of the receptor make these molecules very attractive to study the biological relevance of intracellular GPCRs. Up to date, several photo-activable probes with subcellular targeting have been developed, although no examples have been reported for GPCRs. In contrast, this strategy has been widely applied to release lipids in specific cell compartments, including the mitochondria-targeted caged sphingosine (Feng et al., 2018), demonstrating the importance of the subcellular location on sphingolipid metabolism and signaling. Another relevant example is the lysosome-targeting caged sphingosine (Feng et al., 2019), which successfully accumulated inside the lysosomes of living cells due to the presence of a morpholine moiety. This caged compound allowed the study of the role of lysosomal sphingosine metabolism in the Niemann-Pick type C1, a neurodegenerative disease characterized by a dysfunction in lysosomal storage. In addition, Wagner et al. developed a family of coumarin-based derivatives of lipid messengers with specific targeting to different organelles, including the previously mentioned mitochondria and lysosomes, as well as plasma membrane and endoplasmic reticulum (Wagner et al., 2018). Selective accumulation in the two last cellular compartments was achieved by the attachment of the negatively-charged sulfonate group and a perfluorinated moiety, respectively. Interestingly, selective uncoupling of individual mitochondria within cells was achieved by using a photo-activatable mitochondria-targeted probe (Chalmers et al., 2012). Although subcellular-targeting molecules have not been used for GPCRs, the existence of chemical moieties that selectively drive a molecule in a

specific intracellular location can easily increase the number of ligands targeting intracellular receptors in a more precise and selective manner.

Overall, we have developed a photo-activable molecule that selectively accumulates in the mitochondrial matrix and that is able to activate melatonin receptors upon light application. **MCS-1145** is presented as a tool of particular interest for the study of melatonin receptor activation, and more precisely, to understand the role of mitochondrial MT_1 receptors as demonstrated by our respiration experiments on isolated mitochondria.

Significance

G protein-coupled receptors (GPCRs) are major membrane receptors and drug targets that are involved in the transduction of extracellular signals into the cell. Emerging evidence supports the ability of GPCRs to promote also signaling from intracellular compartments as diverse as endosomes, the Golgi, mitochondria and the nuclear membrane.

Our study focuses on the function of GPCRs located in mitochondria and the development of pharmacological tools to activate mitochondrial GPCR in a precise spatial and temporal manner. By using the melatonin MT_1 receptor as model GPCR, we show that activation of this receptor directly in mitochondria inhibits mitochondrial respiration. This was observed with exogenous melatonin and melatonin generated by the light-induced uncaging of a photo-activatable melatonin receptor ligand attached to a triphenylphosphonium cation moiety for mitochondrial targeting. Beyond its role in MT_1 receptor, MCS-1145 is a photopharmacological tool which can serve also to study the role of mitochondrial melatonin in many other metabolic and cellular pathways with a high spatiotemporal control and to decipher the multiple roles of this pleiotropic hormone in biology and physiology.

This study represents a significant advance in our understanding of the specific role of mitochondrial GPCRs directly on cellular energy homeostasis by regulating mitochondrial respiration. The ligand synthesis strategy can be readily transposed to other GPCRs suspected to be located in mitochondria or other subcellular compartments.

Acknowledgements

This work was supported by Agence Nationale de la Recherche (ANR-19-CE16-0025-01 « mitoGPCR » to R.J.) and ANR-19-CE14-JCJC to L.B. Institut National de la Santé et de la Recherche Médicale (INSERM), Centre National de la Recherche Scientifique (CNRS). R.J. was supported by the Fondation de la Recherche Médicale (Equipe FRM DEQ20130326503), and ANR-21-CE18-00XX « alloGLP1R » and La Ligue Contre le Cancer N/Ref: RS19/75-127. G.S.B. was supported by a doctoral fellowship from the Fondation de la Recherche Médicale (FRM grant number ECO20170637544) obtained by R.J. This work was supported by Ministerio de Ciencia e Innovación, Agencia Estatal de Investigación and ERDF-FEDER European Fund A way of making Europe, European Union (projects CTQ2017-89222-R and PID2020-120499RB-I00) to A.L. and by the Catalan government (2017 SGR 1604) to A.L. We thank Carolina Cera (SimChem, IQAC-CSIC, Barcelona) for support in the synthesis and analysis of compounds.

Author contributions

Conceptualization, A.L., G.M. and R.J.; Chemical synthesis, G.S.B., L.M., C.S.; Biochemical investigations, G.S.B., A.P.Z., R.Z., L.B, B.M., A.A, A.C., A.O.; Writing – Original Draft, Review and Editing, G.S.B., L.B., A.L., and R.J.; Funding Acquisition, A.L., L.B. and R.J.

Competing Interest

The authors declare no competing interest.

STAR Methods

KEY RESSOURCES TABLE

RESSOURCE AVAILABILITY

Lead Contact

Further information and requests for resources and reagents should be directed to and will be fulfilled by the lead contact, Ralf Jockers (ralf.jockers@inserm.fr).

Material availability

All chemical synthesis procedures and main characterization data are provided in the Organic Synthesis section of the STAR Methods. Additional characterization data are provided in the Compound Characterization Spectra of the Supplemental Information. Antibodies, reagents and cell lines used for biological studies were obtained from commercial or internal sources described in the key resources table. Material generated in this study are available upon request and MTA agreement.

Data and code availability

- Section 1: Data. This paper does not report original datasets. Software used for the biological studies and data analyses were obtained from commercial sources described in the key resources table. All data reported in this paper will be shared by the lead contact upon request.
- Section 2: Code. This paper does not report original code.
- Section 3: Any additional information required to reanalyse the data reported in this paper is available from the lead contact upon request

METHOD DETAILS

Organic synthesis

All chemicals and solvents were obtained from commercial sources and used without purification, except anhydrous solvents, which were previously treated with a system of solvent purification (*PureSolv-EN*™), degassed by purging with inert gases and dried over molecular sieves. Reactions were monitored by thin layer chromatography (TLC) on silica gel (60 F, 0.2 mm, ALUGRAM Sil G/UV_{254} *Macherey-Nagel*) by visualization under 254 and/or 365 nm lamp. Compounds without chromophores were visualized using ethanolic solution of phosphomolybdic acid by heating. Alternatively, Nuclear Magnetic Resonance (NMR) was also used as a technique for reaction monitoring. When purification was required, *flash* column chromatography was performed on silica-gel 60 (Panreac, 40-63 microns RE). Reversed-phase column *flash* chromatography was done on silica-gel C18 (SNAP KP-C18-HS, 50µ, *Biotage*) and automated with *Isolera™ One* with UV-Vis detection (*Biotage*).

Compound characterization by NMR spectroscopy was performed with *Variant-Mercury 400 MHz* spectrometer. Chemical shifts δ are reported in parts per million (ppm) from tetramethylsilane as internal standard and using residual non-deuterated solvent signal as reference (Chloroform-*d* δ = 7.26 ppm (^{1}H), δ = 77.16 ppm (^{13}C); Methanol-d_4 δ = 4.87 ppm, δ = 3.31 ppm (^{1}H), δ = 49.3 ppm (^{13}C). The following abbreviations were used to designate

multiplicities: s=singlet, d=doublet, t=triplet, q=quartet, m=multiplet, q=quintuplet, br=broad, dd=double-doublet, ddd=double-double-doublet, dt=double-triplet, td=triple-doublet. Coupling constants (*J*) were expressed in Hz. Signals were assigned as far as possible by means of two-dimensional NMR spectroscopy: ^{1}H-^{1}H-COSY, HSQC and HMBC.

Purity of compounds were determined by HPLC using two different methods (Method A and Method B). In both cases, purity is given as % of absorbance at 254 nm.

Method A uses a *Dionex Ultimate 3000SD* HPLC (*Thermo Fischer Scientific*), which is coupled to a PDA detector and to a mass spectrometer *LTQ XL ESI-ion trap* (*Thermo Fischer Scientific*). For this method, the column used was *ZORBAX Extend C18* (2.1 x 50 mm, 3.5 µm; P.N. 735700-902). The flow rate was 0.9 mL/min, column temperature was fixed to 30 ºC and total runtime was 10 min. The mobile phase used was a mixture of A = formic acid 0.05% in water and B = formic acid 0.05% in ACN, with the method described as follows: from 5% of B to 90%B in 5 min, 90% of B for 2 min, from 90% of B to 100% of B in 1 min and 100% of B for 2 min. UV-Vis spectra were collected every 0.2 s between 190 and 800 nm and bands are % of maximal absorbance. Data from mass spectra were analyzed by electrospray ionization in positive and negative mode between 50 and 2000 Da, using Xcalibur software version 2.2 (*Thermo Fischer Scientific*).

Method B uses a *Waters2795 Alliance* HPLC, coupled to a DAD detector (*Agilent 1100*) and to an ESI *Quattro micro* MS detector (*Waters*). For this method, column used was *ZORBAX Eclipse Plus C18* (4.6 x 150 mm, 3.5 µm). The flow rate was 0.5 mL/min, column temperature was fixed to 35 ºC and total runtime was 10 min. The mobile phase used was a mixture of A = formic acid 0.05% in water and B = formic acid 0.05% in acetonitrile (ACN), with the method described as follows: 5% of B for 0.5 min, from 5% B to 100% B in 5 min, 100% of B for 1.5 min, from 100% of B to 5% of B in 1 min, and 5% of B for 2 min. UV-Vis spectra were collected every 0.2 s between 210 and 600 nm and bands are % of maximal absorbance. Data from mass spectra were analyzed by electrospray ionization in positive and negative mode every 0.3 s between 150 and 1500 Da, using MassLynx software version 4.1 (*Waters*).

High-resolution mass spectra (HRMS) and elemental composition were analyzed by FIA (Flux Injected Analysis) using Ultrahigh-Performance Liquid Chromatography (UPLC) *Aquity (Waters)* coupled to LCT Premier Orthogonal Accelerated Time of Flight Mass Spectrometer (TOF-MS) (*Waters*). Data from mass spectra were analyzed by electrospray ionization in positive and negative mode using MassLynx software version 4.1 (*Waters*). Spectra were scanned between 50 and 1500 Da with values every 0.2 s and peaks are given in m/z. Melting points were taken on open capillary tubes and measured with Melting Point B-545 (*Büchi*),

ramp 0.5 °C/min with a digital temperature measurement. IR spectra were registered in chloroform solution and recorded using *Thermo Nicolet Avatar 360 FT-IR* Spectrometer.

4-(benzyloxy)-3-methoxybenzaldehyde (2): commercially available vanillin **(1)** (8.52 g, 56 mmol, 1 eq) and potassium carbonate (3.91 g, 28 mmol, 0.5 eq) were purged under a nitrogen atmosphere and solved in anhydrous DMF (60 mL, 0.9 M). The reaction mixture was stirred for 1 hour at RT and benzyl bromide (12.30 mL, 101 mmol, 1.8 eq) was added dropwise. All reagents were stirred for 1 hour at RT and then over weekend at 85 ºC. After, the reaction mixture was cooled to RT and 100 mL of water were added. The organic layer was washed with brine (3 x 40 mL) to eliminate DMF, and the organic layers were combined, dried over anhydrous $MgSO_4$, filtered and evaporated under reduced pressure. The resulting crude was first purified by column chromatography on silica using hexane/EtOAc (7:3). The product-containing fractions were recrystallized from ethanol to give the expected product as white crystals (8.5 g, 62%). ^{1}H and ^{13}C-NMR were in good agreement with those described in the literature (Lai et al., 2016). ^{1}H-NMR (400 MHz, Chloroform-*d*): δ = 9.83 (s, 1H), 7.47 – 7.27 (m, 7H), 6.98 (d, J = 8.2 Hz, 1H), 5.23 (s, 2H), 3.93 (s, 3H). ^{13}C-NMR (101 MHz, Chloroform-*d*): δ = 190.97, 153.67, 150.14, 136.09, 130.37, 128.79 (2C), 128.28, 127.29 (2C), 126.65, 112.47, 109.44, 70.93, 56.12. HPLC-PDA-MS (using method A): t_R = 2.70 min, l_{max} = 236, 264, 300 nm; purity 97% (254 nm).

4-(benzyloxy)-5-methoxy-2-nitrobenzaldehyde (3): to an ice-cooled solution of 4-(benzyloxy)-3-methoxybenzaldehyde **(2)** (5.57 g, 23 mmol, 1 eq) in glacial acetic acid (70 mL, 0.3 M) under a nitrogen atmosphere, nitric acid (10.5 mL, 161 mmol, 7 eq) was added dropwise. The reaction mixture was then stirred temperature for 4 days at RT. Afterwards, the reaction was cooled to 0 ºC and a solution of NH_3 (30% w/w, 100 mL) was added carefully into the mixture until basic pH. The mixture was then extracted with DCM (5 x 60 mL) and the combined organic phase was dried over anhydrous $MgSO_4$, filtered and evaporated under reduced pressure. The crude was then purified by column chromatography on silica eluting hexane/EtOAc (3:1), giving the desired product as a yellow solid (3.5 g, 51%). ^{1}H-NMR and ^{13}C were in good agreement with those described in the literature (Lai et al., 2016). ^{1}H-NMR (400 MHz, Chloroform-*d*): δ = 10.44 (s, 1H), 7.67 (s, 1H), 7.50 – 7.34 (m, 6H), 5.28 (s, 2H), 4.02 (s, 3H). ^{13}C-NMR (101 MHz, Chloroform-*d*): δ = 187.89, 153.87, 151.55, 134.97, 129.06, 129.02, 128.86, 127.72, 127.69, 125.87, 110.17, 109.05, 71.72, 56.88, 31.08. HPLC-PDA-MS (using method A): t_R = 2.88 min, l_{max} = 232, 263, 307, 344 nm; purity 86% (254 nm).

4-hydroxy-5-methoxy-2-nitrobenzaldehyde (4): 4-(benzyloxy)-5-methoxy-2-nitrobenzaldehyde **(3)** (3.40 g, 11.25 mmol, 1 eq) was purged under nitrogen and dissolved in 2,2,2-trifluoroacetic acid (43.5 mL, 563 mmol, 50 eq). The yellow solution was stirred for four days at RT. The reaction mixture was then evaporated under reduced pressure, and the crude was rinsed several times with hexane until complete removal of the solvent. The crude product was purified by column chromatography on silica using hexane/EtOAc (3:2), giving the desired compound as a yellow solid (1.60 g, 71%). ^{1}H-NMR and ^{13}C-NMR were in good agreement with those described in the literature (Lai et al., 2016). ^{1}H-NMR (400 MHz, Chloroform-*d*): δ = 10.40 (s, 1H), 7.68 (s, 1H), 7.46 (s, 1H), 6.25 (s, 1H), 4.07 (s, 3H). ^{13}C-NMR (101 MHz, Chloroform-*d*): δ = 187.62, 150.49, 149.80, 145.16, 125.15, 111.36, 109.89, 57.04. HPLC-PDA-MS (using method A): t_R = 1.91 min, l_{max} = 233, 264, 308, 347 nm; purity 95% (254 nm).

4-(hydroxymethyl)-2-methoxy-5-nitrophenol (5): to an ice-cooled solution of 4-hydroxy-5-methoxy-2-nitrobenzaldehyde **(4)** (1.57 g, 7.96 mmol, 1 eq) in ethanol (45 mL, 0.2 M) under a nitrogen atmosphere, sodium borohydride (1.57 g, 39.80 mmol, 5 eq) was added portionwise. The reaction mixture rapidly turned red, and it was stirred overnight at RT. The reaction was quenched with water (10 mL) at 0 ºC, and the mixture was extracted by ethyl acetate (3 x 50 mL). Combined organic layers were washed with brine (2 x 50 mL), dried over anhydrous $MgSO_4$, filtered and evaporated under reduced pressure. The desired compound was obtained without further purification as a dark yellow solid (1.70 g, 95%). ^{1}H and ^{13}C NMR were in good agreement with those described in the literature (Lai et al., 2016). ^{1}H-NMR (400 MHz, Methanol-d_4): δ = 7.60 (s, 1H), 7.37 (s, 1H), 4.93 (s, 2H), 3.99 (s, 3H). ^{13}C-NMR (101 MHz, Methanol-d_4): δ = 154.06, 146.66, 140.73, 132.96, 112.72, 110.92, 62.24, 56.72. HPLC-PDA-MS (using method A): t_R = 1.46 min, l_{max} = 244, 307, 352 nm; purity 94% (254 nm).

(4-(3-bromopropoxy)-5-methoxy-2-nitrophenyl)methanol (6): to a previously stirred suspension of 4-(hydroxymethyl)-2-methoxy-5-nitrophenol **(5)** (1.10 g, 5.52 mmol, 1 eq) and potassium carbonate (1.91 g, 13.81 mmol, 2.5 eq) in acetone (40 mL, 0.1 M), 1,3-dibromopropane (2.30 mL, 22.09 mmol, 4 eq) was added dropwise at RT. The resulting mixture was heated under reflux overnight with magnetic stirring. Then, the reaction was cooled down to RT and the potassium carbonate was filtered off and washed several times with acetone (3 x 15 mL). The filtrated was evaporated under reduced pressure and the resulting crude was partitioned between diethyl ether (50 mL) and water (30 mL). The aqueous layer was extracted with diethyl ether (3 x 30 mL) and the organic layers were combined, dried over $MgSO_4$, filtered and evaporated under reduced pressure. The crude product was purified by column

chromatography through silica gel using Et_2O/Hexane (3:1) to yield the desired product as a pale orange solid (1.24 g, 70%). ^{1}H and ^{13}C-NMR were in good agreement with those described in the literature (Paul et al., 2016). ^{1}H-NMR (400 MHz, Chloroform-*d*): δ = 7.73 (s, 1H), 7.17 (s, 1H), 4.96 (s, 2H), 4.22 (t, *J* = 5.9 Hz, 2H), 3.98 (s, 3H), 3.63 (t, *J* = 6.4 Hz, 2H), 2.40 (q, *J* = 6.1 Hz, 2H). ^{13}C-NMR (101 MHz, Chloroform-*d*): δ = 154.47, 147.23, 139.79, 132.70, 111.42, 109.96, 67.10, 62.98, 56.55, 32.13, 29.74. HPLC-PDA-MS (using method A): t_R = 2.46 min, l_{max} = 210, 220, 242, 309, 347 nm; purity 93% (254 nm).

1-(bromomethyl)-4-(3-bromopropoxy)-5-methoxy-2-nitrobenzene (7): to an ice-cooled solution of (4-(3-bromopropoxy)-5-methoxy-2-nitrophenyl)methanol **(6)** (540 mg, 1.69 mmol, 1 eq) in dry DCM (17 mL, 0.1 M) under an inert atmosphere, tribromophosphine (324 µL, 3.37 mmol, 2 eq) was added dropwise, and the solution was stirred overnight at RT. The reaction was quenched with a saturated solution of $NaHCO_3$ until neutral pH, and the aqueous layer was extracted with DCM (30 mL x 4). The organic phases were combined, washed with brine (2 x 30 mL), dried over $NaSO_4$, filtered and evaporated under reduced pressure, giving the desired product as orange crystals (375 mg, 58%). ^{1}H-NMR and ^{13}C-NMR were in good agreement with those described in the literature (Paul et al., 2016). ^{1}H-NMR (400 MHz, Chloroform-*d*): δ = 7.70 (s, 1H), 6.94 (s, 1H), 4.86 (s, 2H), 4.22 (t, *J* = 5.8 Hz, 2H), 3.97 (s, 3H), 3.63 (t, *J* = 6.3 Hz, 2H), 2.40 (p, *J* = 6.1 Hz, 2H). ^{13}C-NMR (101 MHz, Chloroform-*d*): δ = 153.72, 148.19, 140.26, 127.83, 114.06, 110.14, 67.06, 56.61, 32.05, 30.21, 29.63. HPLC-PDA-MS (using method A): t_R = 3.02 min, l_{max} = 253, 312, 346 nm; purity 93% (254 nm).

N-(2-(1-(4-(3-bromopropoxy)-5-methoxy-2-nitrobenzyl)-5-methoxy-1H-indol-3-yl)ethyl) acetamide (8): to an ice-cooled suspension of sodium hydride (20 mg, 0.42 mmol, 0.9 eq) in dry DMF (2.5 mL, 0.2 M) under an inert atmosphere, a solution of commercially available melatonin (110 mg, 0.46 mmol, 1 eq) in dry DMF (0.8 mL, 0.6 M) was added dropwise. The ice/water bath was then removed, and the mixture was stirred at RT for 1.5 hours. After, the reaction was cooled down to -55 ºC and protected from light exposure with aluminum foil. A previously cooled solution of 1-(bromomethyl)-4-(3-bromopropoxy)-5-methoxy-2-nitrobenzene **(7)** (192 mg, 0.50 mmol, 1.1 eq) in dry DMF (6 mL, 0.1 M) at -55 ºC was added rapidly into the reaction mixture. The mixture was stirred for 4 hours at a temperature below 5-10 ºC, and then quenched with ice-cooled MeOH (20 mL). The resulting solution was evaporated under reduced pressure without heating the water bath to remove the maximum proportion of DMF. The obtained brown residue was partitioned between water (30 mL) and EtOAc (40 mL), and the organic phase was washed with brine (50 mL x 2). The aqueous layers were extracted with

EtOAc (3 x 30 mL) and the organic phases were combined, dried over $MgSO_4$, filtered and concentrated under reduced pressure. The crude product was first purified by column chromatography through silica gel using DCM/MeOH (95:5), to rapidly discard the numerous undesired sub-products from the benzyl bromide. Then, the product-containing fractions were purified again by column chromatography through silica gel using DCM/MeOH (97:3) to yield the expected N-(2-(1-(4-(3-bromopropoxy)-5-methoxy-2-nitrobenzyl)-5-methoxy-1H-indol-3-yl)ethyl) acetamide as a pale brown solid (19.5 mg, 9%).

^{1}H-NMR (400 MHz, Chloroform-*d*): δ = 7.77 (s, 1H), 7.07 (d, *J* = 2.4 Hz, 1H), 7.04 (d, *J* = 8.9 Hz, 1H), 6.95 (s, 1H), 6.84 (dd, *J* = 8.9, 2.4 Hz, 1H), 5.80 (s, 1H), 5.67 (s, 2H), 5.62 (s, 1H), 4.19 (t, *J* = 5.8 Hz, 2H), 3.86 (s, 3H), 3.58-3.53 (m, 4H), 3.42 (s, 3H), 2.96 (t, *J* = 6.9 Hz, 2H), 2.36 (p, *J* = 6.1 Hz, 2H), 1.95 (s, 3H). ^{13}C-NMR (101 MHz, Chloroform-*d*): δ = 170.27, 154.47, 154.40, 147.22, 139.40, 132.23, 129.86, 128.57, 127.06, 112.81, 112.75, 110.75, 110.02, 109.98, 101.05, 67.05, 56.13, 56.03, 48.24, 40.13, 32.07, 29.70, 25.50, 23.53. HPLC-PDA-MS (using method A): t_R = 2.86 min, l_{max} = 224, 281, 305, 342 nm; purity 92% (254 nm). HRMS calculated for $C_{24}H_{29}BrN_3O_6$: 534.1240 $[M+1]^+$, found: 534.1237. Melting point: 192.3-192.4 ºC. IR ($CDCl_3$) v (cm^{-1}) = 3053, 2934, 1661 (C=O stretching), 1520 (N-O stretching), 1486, 1265 (C-O stretching), 1215 (C-O stretching), 732, 702 (C-Br stretching).

(3-(4-((3-(2-acetamidoethyl)-5-methoxy-1H-indol-1-yl)methyl)-2-methoxy-5-nitrophenoxy)propyl) triphenylphosphonium (MCS-1145): to a stirred solution of N-(2-(1-(4-(3-bromopropoxy)-5-methoxy-2-nitrobenzyl)-5-methoxy-1H-indol-3-yl)ethyl) acetamide **(8)** (48 mg, 0.09 mmol, 1 eq) in ACN (2 mL, 0.05 M) under nitrogen, a solution of triphenylphosphine (72 mg, 0.27 mmol, 3 eq) in ACN (0.9 mL, 0.3 M) was added at RT. The mixture was then heated under reflux for two days with magnetic stirring. The reaction was then cooled down to RT and added into a rapidly stirred diethyl ether (15 mL). The yellow precipitate was filtered off and re-dissolved in the minimum volume of DCM (4 mL). This new solution was added again into a rapidly stirred diethyl ether (15 mL). The precipitate was filtered off and the whole process was repeated twice, to yield the final product as a pale yellow solid (48 mg, 75%).

^{1}H-NMR (400 MHz, Methanol-d_4): δ = 8.11 (s, 1H), 7.88 – 7.81 (m, 9H), 7.76 – 7.70 (m, 7H), 7.16 (d, *J* = 2.4 Hz, 1H), 7.13 (s, 1H), 7.09 (d, *J* = 8.9 Hz, 1H), 6.79 (dd, *J* = 8.8, 2.4 Hz, 1H), 5.86 (s, 1H), 5.67 (s, 2H), 4.21 (t, *J* = 5.3 Hz, 2H), 3.84 (s, 3H), 3.66 – 3.58 (m, 2H), 3.48 (t, *J* = 7.0 Hz, 2H), 3.41 (s, 3H), 2.96 (t, *J* = 7.5 Hz, 2H), 2.24-2.15 (m, 2H), 1.95 (s, 3H). ^{13}C-NMR (101 MHz, Methanol-d_4): δ = 171.79, 154.16, 153.90, 146.30, 139.40, 134.88, 134.85, 133.45, 133.35, 132.05, 130.15, 130.11, 130.02, 128.60, 127.04, 118.70, 117.84, 112.63, 111.87,

110.21, 109.80, 109.67, 100.48, 67.93, 67.79, 55.09, 54.84, 40.04, 24.74, 22.30, 21.28, 18.99, 18.46. HPLC-PDA-MS (using method B): t_R = 3.27 min, l_{max} = 225, 276, 308, 355 nm; purity > 98% (254 nm). HRMS calculated for $C_{42}H_{43}N_3O_6P^+$: 716.2889 [M^+ (phosphonium cation)], found: 716.2891. Melting point: decomposes > 100 ºC. IR (Solid) *v* (cm^{-1}) = 3259 (N-H stretching), 3058, 2937, 1656 (C=O stretching), 1520 (N-O stretching), 1485, 1438, 1330 (C-N stretching), 1274 (C-O stretching), 1215 (C-O stretching), 725 (C=C bending).

Photochemistry

UV-Vis absorption spectra of a 100 μM solution in DMSO of each compound were recorded using the Infinite M1000 Tecan microplate reader (λ = 250 – 800 nm). Irradiation experiments to trigger uncaging were performed in a 96-well white plate using a *BlueClassic* laser (TorLaser, Spain) to irradiate the samples from top (λ = 405 nm, 2.37 mW/mm^2). All samples were prepared with a concentration of 20 μM in phosphate-buffered saline (PBS) buffer, containing 2% DMSO. 200 μL of these solutions were irradiated for different periods of time (t = 0, 3, 5, 8, 10, 15 and 30 min) and then analyzed by HPLC-MS to monitor photolysis. These analyses were performed in a *Dionex Ultimate 3000SD* HPLC (*Thermo Fischer Scientific*), which is coupled to a PDA detector and to a mass spectrometer *LTQ XL ESI-ion trap* (*Thermo Fischer Scientific*). Conditions of the analysis are those for Method A (see Organic Chemistry section). Calibration curves of all quantifiable species were determined in each experiment, by analyzing a minimum of seven dilutions of each compound, prepared at different concentrations ranging from 0.2 to 50 μM. Curves were fit by plotting the peak area of the analyte versus the concentrations of the analyte with least-squares linear regression. All experiments were performed at least in triplicate.

Cell culture

HEK293 cells were grown in complete medium (Dulbecco's modified Eagle's medium supplemented with 10% (v/v) fetal bovine serum (FBS), 4.5g/L glucose, 100 U/mL penicillin, 0.1 mg/mL streptomycin and 1mM glutamine) (Invitrogen, CA, USA). Cells were maintained at 37 ºC (95% O_2, 5% CO_2).

Radioligand binding experiments

Radioligand binding assays were performed in 75 mM Tris (pH 7.4), 12 mM $MgCl_2$, 5 mM EDTA and 2-[^{125}I]-MLT as radioligand (PerkinElmer, Waltham, MA, USA), using membranes extracted from HEK293 cells stably expressing human MT_1 or MT_2 receptors. Saturation

binding experiments were performed in the range of 1-1000 pM, and specific binding was defined as binding displaced by 10 µM melatonin. Competition curves were performed by simultaneous incubation of 200 pm 2-[^{125}I]-MLT and increasing concentrations of the respective ligands. Assays were carried out in duplicates for 2 hours at 37 ºC, followed by a rapid filtration through glass fiber filters (Whatman, Clifton, NJ, USA). Filter-retained radioactivity was determined with a γ-counter LB2111 (Berthold Technologies, Bad Wildbad, Germany). Competition curves were fitted with a one-site non-linear regression to determine IC_{50} values, using GraphPad Prism software version 6.0 (San Diego, CA, USA). Data were represented as percentage of maximal binding in the absence of compounds and normalized to melatonin maximum effect. K_i values were calculated from IC_{50} values using the Cheng-Prussof formula: $K_i = IC_{50}/[1 + (L/K_d)]$, where L represents the 2-[^{125}I]-MLT concentration and K_d the dissociation constant obtained in the corresponding radioligand saturation assays. K_d values were 198 ± 30 and 211 ± 19 pM for MT_1 and MT_2, respectively, obtained from three independent saturation binding experiments.

Crude membrane preparation

Crude membranes were prepared as previously described (Ayoub et al., 2004; Jockers et al., 1996; Work and Work, 1979). Confluent cells were washed with ice-cooled PBS, scrapped off in cold PBS on ice and centrifuged at 1200 rpm for 5 min at 4 ºC. The resulting pellet was resuspended in an aqueous buffer containing 75 mM Tris (pH 7.4) and 5 mM EDTA. Cells were then lysed by sonication using a T25 Ultra-Turrax homogenizer (Janke & Kunkel, IKA Labortechnik, Staufen im Breisgau, Germany) for 15 s (3 cycles of 5 s each, at 20500 min^{-1}) and centrifuged at 20000 rpm for 45 min at 4 ºC. The resulting pellet was resuspended and homogenized in an aqueous buffer containing 75 mM Tris (pH 7.4), 12 mM $MgCl_2$ and 5 mM EDTA. Membranes were divided in several one-use aliquots and stored at -80 ºC. The expression of MT_1 and MT_2 receptors in the crude membranes was quantified by BCA assay, using Pierce™ BCA Protein Assay kit (ThermoFischer Scientific, Whaltham, MA, USA) and following the manufacturer's instructions.

Accumulative cAMP assay

The accumulative cAMP assay was performed as previously described (Kamal et al., 2015), using the CisBio cAMP-G_i kit (Cisbio Bioasays, Codolet, France). Briefly, HEK293 cells transiently expressing MT_1 or MT_2 receptors were dispensed into a 384-well plate (4000 cells per well) and stimulated with 1 µM forskolin in the presence of increasing concentrations of melatonin or the ligands of interest, in PBS buffer supplemented with 1 mM IBMX (Sigma-

Aldrich, St Quentin, France) for 30 min at RT. Cells were then lysed for 1 h at RT, and cAMP levels were determined following the manufacturer's instructions. The plate was read using the Infinite F500 Tecan microplate reader. Data were fitted by non-linear regression to determine E_{max} and EC_{50} values and normalized to forskolin-induced response (100%) using GraphPad Prism software.

Real-time BRET assays for cAMP activity

Cells were transfected with MT_1 and YFP-Epac-RLuc cAMP (CAMYEL) BRET sensor, using JetPEI reagent according to the supplier's instructions (Polyplus-transfection, NY, USA). After 24 h, cells were washed, trypsinized and resuspended in DMEM. 100 µL of the cell suspension were seeded in a 96-well plate, previously coated with poly-lysine. BRET assay was performed the next day as previously described (Masri et al., 2008). Briefly, cells were washed with PBS and treated with 1 µM FSK. Then, 10 µL of coelenterazine h were added to each well at RT, in order to have a final 5 µM concentration. Ligands were added under dark conditions 5 minutes after the addition of the Rluc substrate, and plate was read using the Infinite F500 Tecan microplate reader. For the experiments including a washing step, cells were washed with PBS and treated with the ligands and 1 µM FSK. Then, cells were washed for 5 min and 10 µL of coelenterazine h were added to each well at RT, and the plate was read after 5 minutes of the substrate addition. BRET signal was determined by calculating the ratio of the light emitted at 535 nm over the light emitted at 485 nm. BRET data represent the mean ± S.E.M. of at least three independent experiments. For time-courses, data were normalized as a percentage of the maximum melatonin effect and were plotted against time. Concentration-response curves were generated by fitting non-linear regressions to data at 15 minutes, in order to determine EC_{50} values, and normalized to melatonin maximal effect (100%) using GraphPad Prism software.

Immunofluorescence microscopy

Non-transfected HEK293T cells were plated on a 24-well plate ($5x10^4$ cells per well), with glass cover slips and previously coated with poly-L-lysine. Cells were maintained overnight at 37°C, 5% CO_2. Cells were incubated for 15 min under dark conditions with the vehicle or 100 nM of ligand (melatonin or the compounds MCS-0382 or MCS-1145). Then, cells were washed with PBS and fixed in 2% paraformaldehyde for 10 min at RT, and washed three times with PBS for 5 min. Cells were permeabilized with 0.1% TritonX-100 for 5 min, and washed three times with PBS for 5 min. Then, the non-specific sites were blocked with 5% horse serum in PBS with 0.1% Tween for 1 h. Cells were then incubated with rabbit anti-melatonin antibody

(Abbexa, Cambridge, United Kingdom) for 1 h at RT, diluted in PBS with 0.1% Tween and 5% horse serum to a 5 µg/mL final concentration. After three washes with PBS for 5 min each one, cells were incubated with the donkey anti-rabbit secondary antibody (Invitrogen™, Thermofisher Scientific, Massachusetts, USA) for 1 h at RT, diluted 1:800 in PBS with 0.1% Tween and 5% horse serum. Then, cells were washed three times with PBS for 5 min, and incubated with the anti-TOMM20 antibody for 45 min (Alexa Fluor, Abcam, Cambridge, UK), diluted 1:1000 in PBS with 0.1% Tween, 1% BSA and 5% horse serum, and finally with DAPI for 5 min, diluted 1:1000 in PBS (Santa Cruz Biotechnology, Dallas, TX, USA), in order to stain the cell nuclei. Then, cells were washed twice with PBS for 5 minutes and the slides were mounted using a glycergel mounting medium (Dako, Agilent, USA) and analyzed by fluorescence microscopy. Images were acquired under 100×oil objective using specific excitation/emission filters to image the Anti-melatonin antibody (ex: 491 nm), TOMM20 (ex: 647 nm) and DAPI (ex: 405 nm). Images were analyzed using ImageJ software (National Institutes of Health, USA).

Colocalization was assessed by measuring the fractional overlap in at least three different images, between the staining of the anti-melatonin antibody and the staining of the mitochondrial marker TOMM20. This was calculated with the Manders' Colocalization Coefficient analysis using the JACoP plugin for ImageJ.

Mitochondria preparation

HEK293 cells were transfected with MT_1, MT_2 or GFP, using JetPEI reagent according to the supplier's instructions (Polyplus-transfection, NY, USA). Then, they were collected, resuspended in ice-cold isolation buffer (70 mM sucrose, 210mM Mannitol, 50 mM Tris, 1 mM EDTA, pH 7.4) and disrupted with 25 strokes using a 25G needle. The total cell lysate was centrifuged at 800 g at 4 °C, in order to remove cell debris and nuclei. The supernatant was kept and centrifuged at 6900 g for 10 min at 4 °C. The obtained supernatant corresponded to the cytosolic fraction, the pellet was resuspended and the last centrifugation cycle was repeated. The last pellet corresponded to the mitochondrial fraction. All the experiments requiring isolated mitochondria were performed within 3 h after purification.

Oxygen consumption experiments on isolated mitochondria

The oxygen consumption of isolated mitochondria was monitored using the Oxygraph-2k (Oroboros Instruments, Austria). Purified mitochondria (75-100 µg) were suspended in 2 mL of MIRO5 respiration buffer (Long et al., 2019) and added in one of the cuvettes of the

Oxygraph-2k. Respiratory substrates pyruvate (5 mM), malate (2 mM) and glutamate (10mM) were successively added to measure basal respiration, before adding the ligands or the vehicle. Then ADP (5 mM) was added to stimulate Complex-I dependent respiration. Effects of ligand was monitored and expressed in percentage of Vehicle or no light control (see after).

Illumination experiments

In order to study the binding affinity and functional properties under light conditions, solutions of the compounds were prepared in aqueous buffer, with concentrations ranging from 10 to 30 µM. 250 µL of solution were deposited in a 96-well white plate and light was applied from top of each well individually, using the same laser source as for the uncaging experiments (see above). Immediately after illumination, the compound was added to the cell system. All the experiments were performed in the dark. For the real-time BRET-based assays, the ligands were not uncaged previously. Therefore, the plate was removed of the plate reader at a specific time point and 20 s of light application were applied to each well from top, using the same laser. For the mitochondrial respiration experiments, isolated mitochondria were illuminated directly in the measuring cuvette for 5 minutes, using the laser as the light source.

Detection of compounds in mitochondria samples by HPLC-MS

Chromatographic and mass spectrometric conditions

Chromatographic separations were accomplished on a Zorbax Extend C18 column (2.1 x 50 mm, 3.5 µm, Agilent) with a Zorbax Extend C18 pre-column (2.1 x 12.5 mm, 5 µm, Agilent). HPLC analysis was performed on a Thermo Scientific Dionex UltiMate 3000 High-Performance Liquid Chromatography system equipped with a pump (LPG-3400SD), an auto-sampler (ACC-3000T) with a thermostated column compartment. The mobile phase consisted of solvent A (water with 0.05% formic acid) and solvent B (acetonitrile with 0.05% formic acid) with a flow rate of 0.9mL/min. The initial mobile phase composition was 5% solvent B, changed progressively to 100% for 3 minutes. Following 3 min under these conditions, then the initial conditions were reinstated within 1 min, and were maintained to allow for column equilibration for 3 min. The column temperature was set to 35 ºC, and the injection volume was 100 µL.

Mass spectrometry detection was carried out on a LTQ XL ion trap mass spectrometer (Thermo Scientific), using ESI source in positive ion mode. Quantification was performed using single reaction monitoring (SRM) mode with the transition on *m/z* 428.5 à 188.0 ± 2, 247 ± 2, 325.2 ± 2, 351.2 ± 2, 369.2 ± 2, 382.1 ± 2, 411.0 ± 2 and 717.2 à 468.2 ± 1 for MCS-1145. The optimal source parameters were as follows: sheath gas flow at 60, aux gas flow at 10, sweep

gas flow at 10, capillary temperature at 300ºC, source voltage at 4.5 kV, capillary voltage at 1 V for MCS-382 and 19V for MCS-1145, and tube lens at 55 V for MCS-382 and 120V for MCS-1145. The compound-dependent parameter normalized collision energy (CE) was set at 25% for MCS-382 and 37% for MCS-1145. System control and data analysis were performed by Thermo Xcalibur 2.2 software (Thermo Scientific).

Calibration curves

The calibration standard curves were obtained from 10 mg/mL stock solutions in DMSO which were diluted MeOH:H_2O (1:1) to get final concentrations in the range 10 µg/mL-0.6 ng/mL. Six-point calibration curves were established with concentrations in the range of 625 ng/mL-2ng/mL for each analyte. Calibration curves were built by plotting the peak area of the analyte versus the concentration (in nM) with weighted ($1/x^2$) least-squares linear regression. The correlation coefficient (R^2) of calibration curves was more than 0.99. The back-calculated concentrations at each point were within ± 20% of theoretical concentrations.

Mitochondria samples extraction

Mitochondria samples were extracted twice by ultrasonication in 500 µL of MeOH:H_2O (4:1) for 20 min. The joined extracts were filtered with a chromafil PET-20/15 MS syringe filter, and the solvent removed at 30 ºC in a vacuum system (GeneVac). Samples were reconstituted in 300 µL of MeOH:H_2O (1:1) and analyzed by HPLC-MS. In the case of MCS-1145, an additional dilution (1/20) was required to obtain peak areas within the linearity range. Final concentrations were calculated by interpolation in the calibration curves and the dilution factors corrected if required.

Data and statistical analysis

The data and statistical analysis comply with the recommendations on experimental design and analysis in pharmacology (Curtis et al., 2018), using GraphPad Prism software. Data are presented as means ± SEM of *n* independent experiments, performed at least in duplicates to ensure the reliability of single values. IC_{50}, EC_{50} and E_{max} values were obtained following non-linear regression (curve fit) with four parameters of data from a minimum of eight different concentrations per experiment, repeated at least three times independently. All assays performed here were previously validated and demonstrated the robustness and variability of the procedure using this number of independent experiments for concentration–response curves. When possible, data were normalized to maximal and minimum responses using melatonin response as a reference in order to avoid unwanted sources of variations, as differences in the amplitude of melatonin effect between independent experiments.

References

Ayoub, M.A., Levoye, A., Delagrange, P., and Jockers, R. (2004). Preferential formation of MT1/MT2 melatonin receptor heterodimers with distinct ligand interaction properties compared with MT 2 homodimers. Mol. Pharmacol. *66*, 312–321. https://doi.org/10.1124/mol.104.000398.

Ayoub, M.A., Landomiel, F., Gallay, N., Jégot, G., Poupon, A., Crépieux, P., and Reiter, E. (2015). Assessing Gonadotropin Receptor Function by Resonance Energy Transfer-Based Assays. Front. Endocrinol. (Lausanne). *6*, 27. https://doi.org/10.3389/fendo.2015.00130.

Bonnefont-Rousselot, D., Collin, F., Jore, D., and Gardès-Albert, M. (2011). Reaction mechanism of melatonin oxidation by reactive oxygen species in vitro. J. Pineal Res. *50*, 328–335. https://doi.org/10.1111/j.1600-079X.2010.00847.x.

Burns, R.J., Smith, R.A.J., and Murphy, M.P. (1995). Synthesis and characterization of thiobutyltriphenylphosphonium bromide, a novel thiol reagent targeted to the mitochondrial matrix. Arch. Biochem. Biophys. *322*, 60–68. https://doi.org/10.1006/abbi.1995.1436.

Cecon, E., Oishi, A., and Jockers, R. (2018). Melatonin receptors: molecular pharmacology and signalling in the context of system bias. Br. J. Pharmacol. *175*, 3263–3280. https://doi.org/10.1111/bph.13950.

Chalmers, S., Caldwell, S.T., Quin, C., Prime, T.A., James, A.M., Cairns, A.G., Murphy, M.P., McCarron, J.G., and Hartley, R.C. (2012). Selective uncoupling of individual mitochondria within a cell using a mitochondria-targeted photoactivated protonophore. J. Am. Chem. Soc. *134*, 758–761. https://doi.org/10.1021/ja2077922.

Chen, D., Mei, Y., Kim, N., Lan, G., Gan, C.L., Fan, F., Zhang, T., Xia, Y., Wang, L., Lin, C., et al. (2020a). Melatonin directly binds and inhibits death-associated protein kinase 1 function in Alzheimer's disease. J. Pineal Res. *69*. https://doi.org/10.1111/jpi.12665.

Chen, M., Cecon, E., Karamitri, A., Gao, W., Gerbier, R., Ahmad, R., and Jockers, R. (2020b). Melatonin MT1 and MT2 receptor ERK signaling is differentially dependent on Gi/o and Gq/11 proteins. J. Pineal Res. *68*, e12641. https://doi.org/10.1111/jpi.12641.

Chuang, D.M., and Costa, E. (1979). Evidence for internalization of the recognition site of β-adrenergic receptors during receptor subsensitivity induced by (-)-isoproterenol. Proc. Natl. Acad. Sci. U. S. A. *76*, 3024–3028. https://doi.org/10.1073/pnas.76.6.3024.

Curtis, M.J., Alexander, S., Cirino, G., Docherty, J.R., George, C.H., Giembycz, M.A., Hoyer, D., Insel, P.A., Izzo, A.A., Ji, Y., et al. (2018). Experimental design and analysis and their reporting II: updated and simplified guidance for authors and peer reviewers. Br. J. Pharmacol. *175*, 987–993. https://doi.org/10.1111/bph.14153.

Dubocovich, M.L., Delagrange, P., Krause, D.N., Sugden, D., Cardinali, D.P., and Olcese, J. (2010). International union of basic and clinical pharmacology. LXXV. Nomenclature, classification, and pharmacology of G protein-coupled melatonin receptors. Pharmacol. Rev. *62*, 343–380. https://doi.org/10.1124/pr.110.002832.

Farley, S., Laguerre, A., and Schultz, C. (2021). Caged lipids for subcellular manipulation. Curr. Opin. Chem. Biol. *65*, 42–48. https://doi.org/10.1016/j.cbpa.2021.04.012.

Feng, S., Harayama, T., Montessuit, S., David, F.P.A., Winssinger, N., Martinou, J.C., and Riezman, H. (2018). Mitochondria-specific photoactivation to monitor local sphingosine metabolism and function. Elife *7*. https://doi.org/10.7554/eLife.34555.

Feng, S., Harayama, T., Chang, D., Hannich, J.T., Winssinger, N., and Riezman, H. (2019). Lysosome-targeted photoactivation reveals local sphingosine metabolism signatures. Chem. Sci. *10*, 2253–2258. https://doi.org/10.1039/C8SC03614D.

Galano, A., Tan, D.X., and Reiter, R.J. (2013). On the free radical scavenging activities of melatonin's metabolites, AFMK and AMK. J. Pineal Res. *54*, 245–257. https://doi.org/10.1111/jpi.12010.
Gbahou, F., Cecon, E., Viault, G., Gerbier, R., Jean-Alphonse, F., Karamitri, A., Guillaumet, G., Delagrange, P., Friedlander, R.M., Vilardaga, J.P., et al. (2017). Design and validation of the first cell-impermeant melatonin receptor agonist. Br. J. Pharmacol. *174*, 2409–2421. https://doi.org/10.1111/bph.13856.
Hansen, M.J., Velema, W.A., Lerch, M.M., Szymanski, W., and Feringa, B.L. (2015). Wavelength-selective cleavage of photoprotecting groups: Strategies and applications in dynamic systems. Chem. Soc. Rev. *44*, 3358–3377. https://doi.org/10.1039/c5cs00118h.
Hegron, A., Huh, E., Deupi, X., Sokrat, B., Gao, W., Le Gouill, C., Canouil, M., Boissel, M., Charpentier, G., Roussel, R., et al. (2021). Identification of Key Regions Mediating Human Melatonin Type 1 Receptor Functional Selectivity Revealed by Natural Variants. ACS Pharmacol. Transl. Sci. *4*, 1614–1627. https://doi.org/10.1021/acsptsci.1c00157.
Hevia, D., Mayo, J.C., Tan, D.X., Rodriguez-Garcia, A., and Sainz, R.M. (2014). Melatonin enhances photo-oxidation of 29, 79-dichlorodihydrofluorescein by an antioxidant reaction that renders N1-acetyl-N2-formyl-5-methoxykynuramine (AFMK). PLoS One *9*. https://doi.org/10.1371/journal.pone.0109257.
Huang, W.Y., Jou, M.J., and Tsung, I.P. (2013). MtDNA T8993G mutation-induced F1F0-ATP synthase defect augments mitochondrial dysfunction associated with hypoxia/reoxygenation: The protective role of melatonin. PLoS One *8*. https://doi.org/10.1371/journal.pone.0081546.
Jiang, L.I., Collins, J., Davis, R., Lin, K.M., DeCamp, D., Roach, T., Hsueh, R., Rebres, R.A., Ross, E.M., Taussig, R., et al. (2007). Use of a cAMP BRET sensor to characterize a novel regulation of cAMP by the sphingosine 1-phosphate/G13 pathway. J. Biol. Chem. *282*, 10576–10584. https://doi.org/10.1074/jbc.M609695200.
Jockers, R., Da Silva, A., Strosberg, A.D., Bouvier, M., and Marullo, S. (1996). New molecular and structural determinants involved in B2-Adrenergic Receptor Desensitization and Sequestration Delineation Using Chimeric B3/B2-Adrenergic Receptors. J. Biol. Chem. *271*, 9355–9362. https://doi.org/10.1074/jbc.271.16.9355.
Jockers, R., Delagrange, P., Dubocovich, M.L., Markus, R.P., Renault, N., Tosini, G., Cecon, E., and Zlotos, D.P. (2016). Update on melatonin receptors: IUPHAR Review 20. Br. J. Pharmacol. 2702–2725. https://doi.org/10.1111/bph.13536.
Johansson, L.C., Stauch, B., McCorvy, J.D., Han, G.W., Patel, N., Huang, X.P., Batyuk, A., Gati, C., Slocum, S.T., Li, C., et al. (2019). XFEL structures of the human MT2 melatonin receptor reveal the basis of subtype selectivity. Nature *569*, 289–292. https://doi.org/10.1038/s41586-019-1144-0.
Jong, Y.J.I., Harmon, S.K., and O'Malley, K.L. (2018). Intracellular GPCRs Play Key Roles in Synaptic Plasticity. ACS Chem. Neurosci. *9*, 2162–2172. https://doi.org/10.1021/acschemneuro.7b00516.
Journé, A.S., Habib, S.A.M., Dodda, B.R., Morcos, M.N.F., Sadek, M.S., Tadros, S.A.A., Witt-Enderby, P.A., Jockers, R., and Zlotos, D.P. (2014). N1-linked melatonin dimers as bivalent ligands targeting dimeric melatonin receptors. Medchemcomm *5*, 792–796. https://doi.org/10.1039/c4md00079j.
Kalliolia, E., Silajdžić, E., Nambron, R., Hill, N.R., Doshi, A., Frost, C., Watt, H., Hindmarsh, P., Björkqvist, M., and Warner, T.T. (2014). Plasma melatonin is reduced in Huntington's disease. Mov. Disord. *29*, 1511–1515. https://doi.org/10.1002/mds.26003.
Kamal, M., Gbahou, F., Guillaume, J.L., Daulat, A.M., Benleulmi-Chaachoua, A., Luka, M., Chen, P., Anaraki, D.K., Baroncini, M., La Cour, C.M., et al. (2015). Convergence of melatonin and serotonin (5-HT) signaling at MT2/5-HT2C receptor heteromers. J. Biol. Chem. *290*, 11537–11546. https://doi.org/10.1074/jbc.M114.559542.

Karamitri, A., Plouffe, B., Bonnefond, A., Chen, M., Gallion, J., Guillaume, J.L., Hegron, A., Boissel, M., Canouil, M., Langenberg, C., et al. (2018). Type 2 diabetes–associated variants of the MT2 melatonin receptor affect distinct modes of signaling. Sci. Signal. *11*. https://doi.org/10.1126/scisignal.aan6622.
Kohl-Landgraf, J., Buhr, F., Lefrancois, D., Mewes, J.M., Schwalbe, H., Dreuw, A., and Wachtveitl, J. (2014). Mechanism of the photoinduced uncaging reaction of puromycin protected by a 6-nitroveratryloxycarbonyl group. J. Am. Chem. Soc. *136*, 3430–3438. https://doi.org/10.1021/ja410594y.
Lai, Y. Sen, Kao, C.L., Chen, Y.P., Fang, C.C., Hu, C.C., and Chu, C.C. (2016). Photodegradable self-assembling PAMAM dendrons for gene delivery involving dendriplex formation and phototriggered circular DNA release. New J. Chem. *40*, 2601–2608. https://doi.org/10.1039/c5nj03173g.
Lin, M.T., and Beal, M.F. (2006). Mitochondrial dysfunction and oxidative stress in neurodegenerative diseases. Nature *443*, 787–795. https://doi.org/10.1038/nature05292.
Lira-Rocha, A., Espejo-González, O., and Naranjo-Rodríguez, E.B. (2002). Receptor-binding studies of 1-N-substituted melatonin analogues. Eur. J. Med. Chem. *37*, 945–951. https://doi.org/10.1016/S0223-5234(02)01410-1.
Liu, J., Clough, S.J., Hutchinson, A.J., Adamah-Biassi, E.B., Popovska-Gorevski, M., and Dubocovich, M.L. (2016). MT1 and MT2 Melatonin Receptors: A Therapeutic Perspective. Annu. Rev. Pharmacol. Toxicol. *56*, 361–383. https://doi.org/10.1146/annurev-pharmtox-010814-124742.
Liu, R.Y., Zhou, J.N., Van Heerikhuize, J., Hofman, M.A., and Swaab, D.F. (1999). Decreased melatonin levels in postmortem cerebrospinal fluid in relation to aging, Alzheimer's disease, and apolipoprotein E-ε4/4 genotype. J. Clin. Endocrinol. Metab. *84*, 323–327. https://doi.org/10.1210/jc.84.1.323.
Long, Q., Huang, L., Huang, K., and Yang, Q. (2019). Assessing mitochondrial bioenergetics in isolated mitochondria from mouse heart tissues using oroboros 2k-oxygraph. In Methods in Molecular Biology, pp. 237–246.
Masri, B., Salahpour, A., Didriksen, M., Ghisi, V., Beaulieu, J.M., Gainetdinov, R.R., and Caron, M.G. (2008). Antagonism of dopamine D2 receptor/β-arrestin 2 interaction is a common property of clinically effective antipsychotics. Proc. Natl. Acad. Sci. U. S. A. *105*, 13656–13661. https://doi.org/10.1073/pnas.0803522105.
Mazzucchelli, C., Pannacci, M., Nonno, R., Lucini, V., Fraschini, F., and Stankov, B.M. (1996). The melatonin receptor in the human brain: Cloning experiments and distribution studies. Mol. Brain Res. *39*, 117–126. https://doi.org/10.1016/0169-328X(96)00017-4.
Melhuish Beaupre, L.M., Brown, G.M., Gonçalves, V.F., and Kennedy, J.L. (2021). Melatonin's neuroprotective role in mitochondria and its potential as a biomarker in aging, cognition and psychiatric disorders. Transl. Psychiatry *11*. https://doi.org/10.1038/s41398-021-01464-x.
Mohammad Nezhady, M.A., Rivera, J.C., and Chemtob, S. (2020). Location Bias as Emerging Paradigm in GPCR Biology and Drug Discovery. iScience *23*. https://doi.org/10.1016/j.isci.2020.101643.
Paul, A., Jana, A., Karthik, S., Bera, M., Zhao, Y., and Singh, N.D.P. (2016). Photoresponsive real time monitoring silicon quantum dots for regulated delivery of anticancer drugs. J. Mater. Chem. B *4*, 521–528. https://doi.org/10.1039/c5tb02045j.
Reiter, R.J., Rosales-Corral, S.A., Tan, D.X., Acuna-Castroviejo, D., Qin, L., Yang, S.F., and Xu, K. (2017). Melatonin, a full service anti-cancer agent: Inhibition of initiation, progression and metastasis. Int. J. Mol. Sci. *18*, 843. https://doi.org/10.3390/ijms18040843.
Reiter, R.J., Tan, D.X., Rosales-Corral, S., Galano, A., Zhou, X.J., and Xu, B. (2018). Mitochondria: Central organelles for melatonins antioxidant and anti-Aging actions. Molecules

23. https://doi.org/10.3390/molecules23020509.
Somalo-Barranco, G., Serra, C., Lyons, D., Piggins, H.D., Jockers, R., and Llebaria, A. (2022). Design and Validation of the First Family of Photo-Activatable Ligands for Melatonin Receptors. J. Med. Chem. https://doi.org/10.1021/ACS.JMEDCHEM.2C00717.
Suofu, Y., Li, W., Jean-Alphonse, F.G., Jia, J., Khattar, N.K., Li, J., Baranov, S. V., Leronni, D., Mihalik, A.C., He, Y., et al. (2017). Dual role of mitochondria in producing melatonin and driving GPCR signaling to block cytochrome c release. Proc. Natl. Acad. Sci. U. S. A. *114*, E7997–E8006. https://doi.org/10.1073/pnas.1705768114.
Tadevosyan, A., Villeneuve, L.R., Fournier, A., Chatenet, D., Nattel, S., and Allen, B.G. (2016). Caged ligands to study the role of intracellular GPCRs. Methods *92*, 72–77. https://doi.org/10.1016/j.ymeth.2015.07.005.
Tan, D.X., Manchester, L.C., Terron, M.P., Flores, L.J., and Reiter, R.J. (2007). One molecule, many derivatives: A never-ending interaction of melatonin with reactive oxygen and nitrogen species? J. Pineal Res. *42*, 28–42. https://doi.org/10.1111/j.1600-079X.2006.00407.x.
Tsvetanova, N.G., Irannejad, R., and Von Zastrow, M. (2015). G protein-coupled receptor (GPCR) signaling via heterotrimeric G proteins from endosomes. J. Biol. Chem. *290*, 6689–6696. https://doi.org/10.1074/jbc.R114.617951.
Viault, G., Poupart, S., Mourlevat, S., Lagaraine, C., Devavry, S., Lefoulon, F., Bozon, V., Dufourny, L., Delagrange, P., Guillaumet, G., et al. (2016). Design, synthesis and biological evaluation of fluorescent ligands for MT1 and/or MT2 melatonin receptors. RSC Adv. *6*, 62508–62521. https://doi.org/10.1039/c6ra10812a.
Vilardaga, J.P., Jean-Alphonse, F.G., and Gardella, T.J. (2014). Endosomal generation of cAMP in GPCR signaling. Nat. Chem. Biol. *10*, 700–706. https://doi.org/10.1038/nchembio.1611.
Wagner, N., Stephan, M., Höglinger, D., and Nadler, A. (2018). A Click Cage: Organelle-Specific Uncaging of Lipid Messengers. Angew. Chemie - Int. Ed. *57*, 13339–13343. https://doi.org/10.1002/anie.201807497.
Wang, B., Zhu, S., Liu, Z., Wei, H., Zhang, L., He, M., Pei, F., Zhang, J., Sun, Q., and Duan, L. (2020). Increased Expression of Colonic Mucosal Melatonin in Patients with Irritable Bowel Syndrome Correlated with Gut Dysbiosis. Genomics, Proteomics Bioinforma. *18*, 708–720. https://doi.org/10.1016/j.gpb.2020.06.013.
Wang, W., Qiao, Y., and Li, Z. (2018). New Insights into Modes of GPCR Activation. Trends Pharmacol. Sci. *39*, 367–386. https://doi.org/10.1016/j.tips.2018.01.001.
Wang, X., Sirianni, A., Pei, Z., Cormier, K., Smith, K., Jiang, J., Zhou, S., Wang, H., Zhao, R., Yano, H., et al. (2011). The melatonin MT1 receptor axis modulates mutant Huntingtin-Mediated Toxicity. J. Neurosci. *31*, 14496–14507. https://doi.org/10.1523/JNEUROSCI.3059-11.2011.
Wongprayoon, P., and Govitrapong, P. (2017). Melatonin as a mitochondrial protector in neurodegenerative diseases. Cell. Mol. Life Sci. *74*, 3999–4014. https://doi.org/10.1007/s00018-017-2614-x.
Work, T.S., and Work, E. (1979). Chapter 2: Methods of cell breakage: Assessing their suitability and efficacy. In Laboratory Techniques in Biochemistry and Molecular Biology, pp. 11–44.
Yang, Y., Duan, W., Jin, Z., Yi, W., Yan, J., Zhang, S., Wang, N., Liang, Z., Li, Y., Chen, W., et al. (2013). JAK2/STAT3 activation by melatonin attenuates the mitochondrial oxidative damage induced by myocardial ischemia/reperfusion injury. J. Pineal Res. *55*, 275–286. https://doi.org/10.1111/jpi.12070.
Zhang, Y., Cook, A., Kim, J., Baranov, S. V., Jiang, J., Smith, K., Cormier, K., Bennett, E., Browser, R.P., Day, A.L., et al. (2013). Melatonin inhibits the caspase-1/cytochrome c/caspase-3 cell death pathway, inhibits MT1 receptor loss and delays disease progression in a mouse

model of amyotrophic lateral sclerosis. Neurobiol. Dis. *55*, 26–35. https://doi.org/10.1016/j.nbd.2013.03.008.
Zielonka, J., Joseph, J., Sikora, A., Hardy, M., Ouari, O., Vasquez-Vivar, J., Cheng, G., Lopez, M., and Kalyanaraman, B. (2017). Mitochondria-Targeted Triphenylphosphonium-Based Compounds: Syntheses, Mechanisms of Action, and Therapeutic and Diagnostic Applications. Chem. Rev. *117*, 10043–10120. https://doi.org/10.1021/acs.chemrev.7b00042.